

PROTAC technology as a Novel tool to identify the target of lathyrane diterpenoids

Yanli Wu^{a,1}, Yueying Yang^{a,1}, Wang Wang^{a,1}, Dejuan Sun^a, Mengzhu Zheng^b, Yingrong Zhou^b, Jing Liang^a, Man Zhu^a, Hua Li^{a,b,*}, Lixia Chen^{a,*}

^a *Wuya College of Innovation, Key Laboratory of Structure-Based Drug Design & Discovery, Ministry of Education, Shenyang Pharmaceutical University, Shenyang, 110016, China.*

^b *Hubei Key Laboratory of Natural Medicinal Chemistry and Resource Evaluation, School of Pharmacy, Tongji-Rongcheng Center for Biomedicine, Tongji Medical College, Huazhong University of Science and Technology, Wuhan, 430030, China.*

¹ These authors contributed equally to this work.

*Corresponding Authors.

E-mail addresses: li_hua@hust.edu.cn (Hua Li), syzycx@163.com (Lixia Chen).

ABSTRACT

Active natural products are an important source of drug discovery due to their unique biocompatibility, novel-structural framework and extensive pharmacological activities. The target identification of natural products is the key to thoroughly understanding their mechanism of action and guiding their subsequent structure optimization. Lathyrane diterpenoids isolated from the seeds of *Euphorbia lathyris* in our laboratory have been proved to possess good anti-inflammatory activities in lipopolysaccharide (LPS)-induced macrophages, but their precise target and mechanism of action remain unclear. Herein, we employed PROTAC technology combined with quantitative proteomic analysis to identify the potential targets of lathyrane diterpenoids in macrophages. ZCY-PROTAC, synthesized based on Lathyrol, the core scaffold structure of the most active natural compound (2*S*,3*S*,4*S*,5*R*,9*S*,11*R*,15*R*)-15-acetoxy-3-cinnamoyloxy-5-hydroxy-14-oxolathyrane-6(17),12*E*-diene, ZCY-001), intensively degraded a target protein MAFF in mouse and human cells. MST, CETSA and DARTS assays confirmed the direct binding of MAFF with Lathyrol or ZCY020, a natural product sharing the same core scaffold structure. Further mechanism studies showed that ZCY020 was capable of inhibiting the formation of a MAFF homodimer, promoting MAFF-Nrf2 heterodimerization, and thus regulating the transcription and expression of downstream protein HO-1, thereby exerting antioxidant, anti-inflammatory activity and promoting protective mitophagy in LPS-induced inflammation in macrophages and acute lung injury in mice. Together, our research indicates that MAFF is a potential target of ZCY020 and other lathyrane diterpenoids, and that PROTAC technology can be an innovative approach and a useful supplement for target identification of natural products.

Keywords: PROTAC, target identification, lathyrane diterpenoids, MAFF, Nrf2, anti-inflammation

INTRODUCTION

Proteolysis Targeting Chimera (PROTAC) is an emerging approach to selectively degrading target proteins by utilizing endogenous proteasome [1,2]. As a heterobifunctional degrader, the PROTAC molecule comprises three parts: a ligand for the cellular protein of interest (POI), an E3 ubiquitin ligase ligand and a linker used for conjugating them [3]. The POI ligand functions by targeting and binding the POI, while the E3 ubiquitin ligase ligand specifically recruits E3 ubiquitin ligase to execute ectopic ubiquitination, leading to POI degradation *via* the ubiquitin-proteasome system [4]. Recently, the employment of E3 ubiquitin ligase such as cereblon (CRBN) in this technology has led to the successful degradation of a variety of target proteins with small-molecule inhibitors [5]. Since PROTACs can degrade target proteins without high affinity, it is natural to speculate that this technology can be used to identify the precise targets of natural products. Natural products are well-characterized to possess pharmacological or biological activities, including anti-inflammatory, anti-oxidant, anti-tumor and anti-fibrotic effects, thus they have attracted great focus on discovering lead compounds and new therapeutic drugs [6]. However, in many cases the biological properties of natural products do not simply arise from the regulation of a single protein or pathway, but are achieved through interaction with a plethora of cellular components [6]. This brings great difficulties for the identification of the exact cellular targets of natural products. Although a recent study reported the employment of PROTACs to explore the unknown non-kinase target of a multi-kinase inhibitor sorafenib, which is widely used in oncotherapy, there were no further researches to verify its precise target and mechanism of action both *in vitro* and *in vivo* [7]. Whether PROTACs can be used to find the potential targets of natural products remains unexplored.

Euphorbia (belonging to Euphorbiaceae), including about 2160 species, is a rich source of special diterpenoids, especially macrocyclic and polycyclic skeletons [8,9]. The seeds of *Euphorbia lathyris* have been widely used as a natural medicine in Asia to treat amenorrhea, terminal schistosomiasis, ascities, snakebites, and hydropsy [10]. Lathyranes, a type of macrocyclic diterpenoids, are characteristic components of *Euphorbia lathyris*. A series of lathyrane diterpenoids have been isolated from the seeds of *Euphorbia lathyris* [11-15] and some of them are known to exert anti-inflammatory activity by inhibiting NF- κ B signaling activation [14-17]. In our previous study, we obtained several new lathyrane diterpenoids from the seeds of *Euphorbia lathyris* and proved their potent anti-inflammatory activity at low micromole levels with low toxicity [14,15]. Among them, (2*S*,3*S*,4*S*,5*R*,9*S*,11*R*,15*R*)-15-acetoxy-3-cinnamoyloxy-5-hydroxy-14-oxolathyrane-6(17),12*E*-diene (ZCY-001) demonstrated the strongest activity against LPS-stimulated NO release with an IC₅₀ value of 3.0 ± 1.1 μ M and exerted inhibition on NF- κ B activation [14]. However, the exact targets and the anti-inflammatory mechanism of lathyrane diterpenoids still need to be elucidated. In view of the good anti-inflammatory activity of lathyrane diterpenoids, we believe it worthy to identify the precise targets of lathyrane diterpenoids to better understand its molecular mechanism in anti-inflammatory therapy.

MAFs family proteins were first identified as basic region leucine zipper (bZIP)-type transcription factors, and can be divided into two groups: large MAFs and small MAFs (sMAFs) [18]. Small Maf proteins consist of MAFF, MAFG and MAFK, and lack transactivation domains [19]. Generally, sMAFs form homodimers or heterodimers with cap 'n' collar (CNC) proteins (p45 NF-E2, Nrf1, Nrf2, and Nrf3) and Bach proteins (Bach1 and Bach2) [20-25]. Since CNC and Bach proteins cannot bind to DNA as monomers, sMAFs are indispensable partners required by CNC and Bach

proteins to bind to the palindromic MAF-recognition element (MARE) (5'-TGCTGACGTCAGCA-3') or to the antioxidant response element (ARE), containing the core sequence, 5'-R(A/G)T(C/G)A(C/T/G)NNNGC-3'. While CNC family members including Nrf2 positive-transcriptionally activate target genes involved in antioxidative response, homodimers of sMafs can play a repressive role in regulating MARE or ARE-dependent genes by competitively binding with MARE or ARE [26,27]. Therefore, the role of sMafs in transcriptional activation or repression is highly dependent on their quantity and the abundance of their binding partners. An increasing number of researches have proved that the transcription and protein levels of MAFF are induced by inflammatory cytokines such as IL-1 β and TNF [28,29], and also by oxidative stress [30], indicating the specific role for MAFF in the cases of oxidative stress and inflammation. Recent research has also reported that under LPS stimulation, MAFF acts as a pro-inflammatory transcription factor [31]. Thus, MAFF can be a potential target for ameliorating oxidative stress and inflammatory responses.

Here, Lathyrol, the core scaffold structure of the most active natural compound ZCY-001, previously isolated from the seeds of *Euphorbia lathyris* [14], was selected to synthesize a PROTAC molecule (ZCY-PROTAC) to identify the targets of lathyrene diterpenoids. Upon the degradation by proteasome, quantitative proteomic analysis was employed to identify the degraded proteins. After the verification of possible targets, we identified MAFF as a dominant target of the core scaffold structure of lathyrene diterpenoids. According to this result, it is certain to speculate that lathyrene diterpenoids may play its anti-inflammatory role through interaction with this target. Among the lathyrene diterpenoids isolated from *Euphorbia lathyris*, (2*S*,3*S*,4*R*,5*R*,7*R*,9*S*,11*R*,15*R*)-5,15-diacetoxy-3-benzoyloxy-7-hydroxy-14-oxolathyrin-6(17),12*E*-diene (ZCY020) showed similar anti-inflammatory activity with ZCY-001 against LPS-induced RAW264.7 cells in our previous studies [14,15]. In this study, we found that ZCY020 can bind directly with MAFF and disrupt the homodimer formation of MAFF, thus significantly inhibiting inflammatory response in RAW264.7 macrophage cells and LPS-induced acute lung injury through the MAFF-Nrf2 pathway. These findings suggest that ZCY020 or lathyrene diterpenoids, as potential MAFF-Nrf2 activators, are capable of relieving inflammation in infectious diseases. This study also implies that PROTAC technology could be a promising new method for the target identification of natural products.

RESULTS

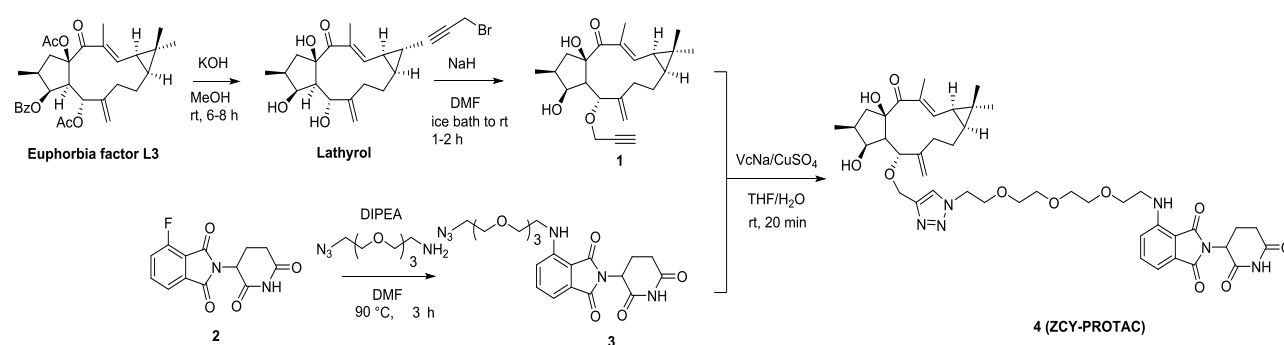
MAFF is a degradation target of ZCY-PROTAC

General synthetic routes of compound ZCY-PROTAC are provided in [Scheme 1](#). To synthesize the PROTAC of lathyrene diterpenoid, Lathyrol, the core scaffold structure of the most active natural compound ZCY-001, was selected as the POI ligand. Lathyrol was obtained by hydrolysis of Euphorbia factor L3 ([Scheme 1](#)) [14], because of its large amount existed in *Euphorbia lathyris* and possessing the same core scaffold structure with ZCY-001 (see [Figure S1](#) for structures). In order to find the anti-inflammation targets of Lathyrol, we first coupled Lathyrol with a 3-polyethylene glycol (3-PEG) linker conjugated to thalidomide (referred to as ZCY-PROTAC, [Figure 1A](#)), and then evaluated its inhibitory effects on LPS-induced nitric oxide (NO) production in RAW264.7 macrophage cells. Compared with Lathyrol, ZCY-PROTAC showed a stronger inhibitory activity against LPS-stimulated NO release ([Figure 1B](#)), while both of them showed only very low toxicity at the indicated dose ([Figure S2](#)). To further investigate the potential targets degraded by

ZCY-PROTAC, a Tandem Mass Tag (TMT)-based quantitative proteomic approach [16,32] was applied to measure the protein fold changes after 48 hours of treatment with 8 μ M ZCY-PROTAC or DMSO in RAW264.7 cells (Figure 1C). A total of 5750 quantifiable proteins were identified in our experiment. According to the protein function, we mapped the proteins related to inflammation with significant differences in protein levels ($p < 0.05$) through a volcano plot (Figure 1D). According to the plot, among these proteins, MAFF was degraded most efficiently, with more than 7 fold decrease in protein level after ZCY-PROTAC treatment compared to the control group (Figure 1D). KEGG pathway enrichment analysis showed that proteins with significant changes in expression levels are mostly related with lysosome, ferroptosis, cholesterol metabolism and mitophagy (Figure 1E), which can be used as a reference for the following mechanism research.

To confirm the degradation of MAFF detected by MS, we used Western blotting to analyze MAFF protein levels in RAW264.7 cells after ZCY-PROTAC treatment. As shown in Figure 1F, MAFF protein was significantly degraded in cells with dose-dependent and time-dependent manners. To further assess MAFF degradation mediated by ZCY-PROTAC in human cells, human HEK293T cell line was selected to be treated with ZCY-PROTAC. As expected, MAFF was degraded by the PROTAC in a concentration-dependent manner. And the degradation of MAFF exhibited time-dependent within 24h (Figure 1G). To exclude the influence of the two ligands of ZCY-PROTAC on MAFF degradation, single Lathryol or thalidomide was administrated and showed no degradation effects on MAFF within 48 h in both RAW264.7 and HEK293T cells (Figure S3A and S3B). And among the sMafs proteins, only the MAFF protein was intensively degraded by ZCY-PROTAC in both RAW264.7 and HEK293T cells in a dose-dependent manner (Figure S3A and S3B), indicating that ZCY-PROTAC has a certain selectivity for the degradation of MAFF.

Furthermore, to determine whether ZCY-PROTAC induces MAFF degradation through the ubiquitin-proteasome system, proteasome inhibitor MG132 was used to block the degradation effect. Western blotting analysis showed that the degradation of MAFF was dose-dependently blocked after pretreatment with MG132 (Figure 1H). Besides, Lathryol and thalidomide were applied to compete with ZCY-PROTAC to bind to MAFF and E3 ubiquitin ligase CRBN. Both Lathryol and thalidomide blocked the degradation of MAFF mediated by ZCY-PROTAC (Figure 1I). These results strongly demonstrate that the degradation of MAFF mediated by ZCY-PROTAC depends on the ubiquitin-proteasome system, and that MAFF is verified to be a novel target of Lathryol-based PROTAC.



Scheme 1. General procedure for ZCY-PROTAC synthesis.

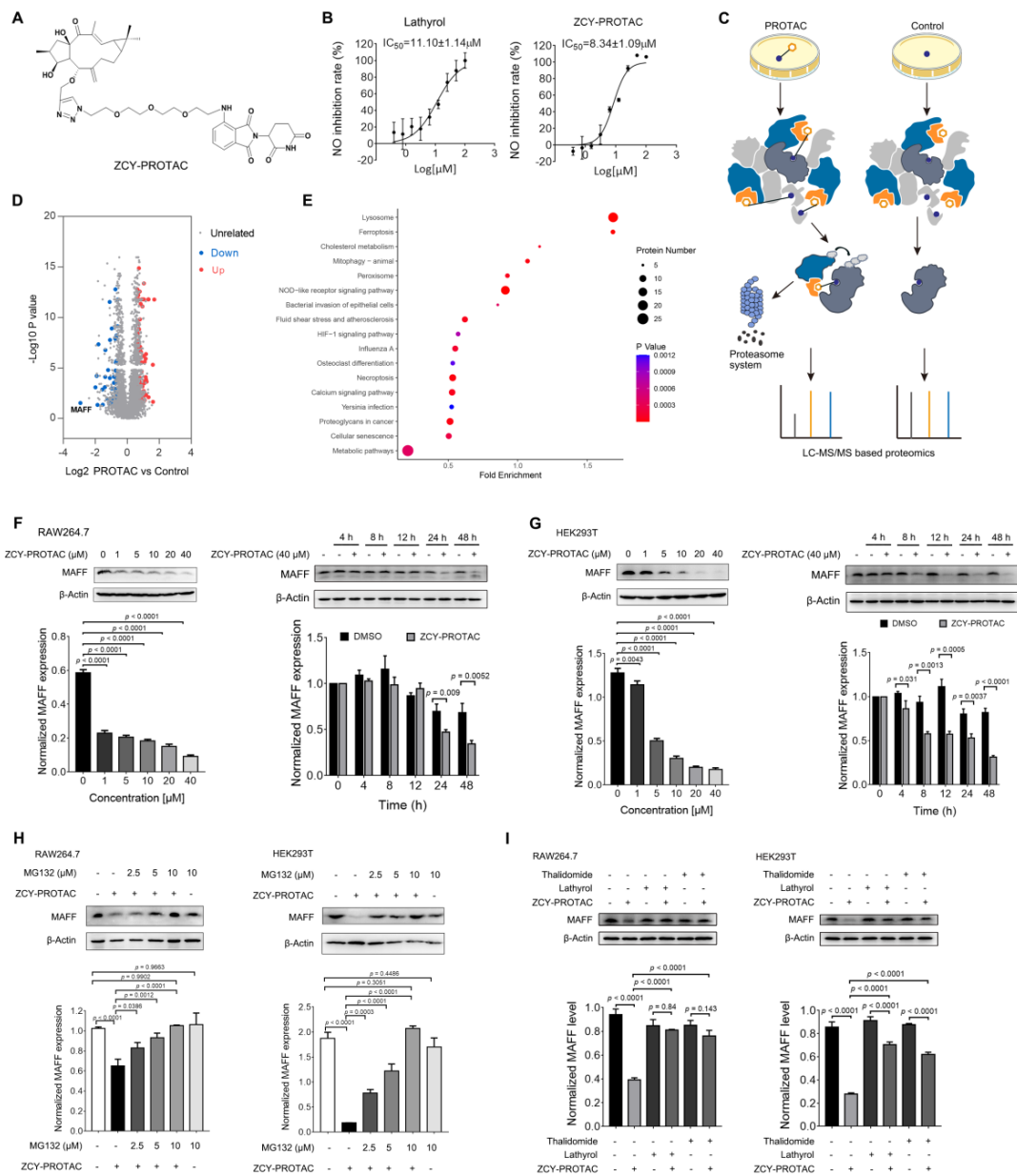


Figure 1. MAFF is a degradation target of ZCY-PROTAC. (A) Structure of Lathyrol-based PROTAC (ZCY-PROTAC). **(B)** The inhibitory effect of Lathyrol and ZCY-PROTAC on NO release induced by LPS in RAW264.7 macrophage cells. $n = 3$. Data are presented as mean \pm SD. **(C)** A Tandem Mass Tags (TMT)-based mass spectrometry (MS) approach was used to assess the proteome changes in RAW264.7 cells after 48 h treatment of ZCY-PROTAC or DMSO control. **(D)** The down-regulated (blue) and up-regulated (red) proteins associated with inflammation were plotted as fold change (ZCY-PROTAC/Control) versus $-\text{Log}_{10}$ of p -value (t -test). **(E)** The fold change of Kyoto Encyclopedia of Genes and Genomes (KEGG) pathway enrichment after 48 h treatment of ZCY-PROTAC or DMSO control. **(F)** Immunoblot analysis of concentration-dependent and time-dependent degradation of MAFF protein in mouse RAW264.7 cells. **(G)** Immunoblot analysis of concentration-dependent and time-dependent degradation of MAFF protein in human HEK293T cells. **(H)** Immunoblot analysis of MAFF protein in RAW264.7 cells and HEK293T cells pre-treated with MG132 for 1 h and subsequently treated with either DMSO or ZCY-PROTAC for 24 h. **(I)** Immunoblot analysis of MAFF protein in RAW264.7 and HEK293T cells treated by ZCY-PROTAC

together with either Lathyrol or Thalidomide for 48 h. Immunoblot analysis data were normalized with β -Actin.

Lathyrol directly binds to MAFF

To further confirm that MAFF is a direct target of Lathyrol (Figure 2A), microscale thermophoresis (MST) assay, cellular thermal shift assay (CETSA) and drug affinity-responsive target stability (DARTS) assay were used to evaluate the ability of Lathyrol binding to MAFF. MST assay was performed to assess the direct binding affinity between Lathyrol and MAFF protein. As shown in Figure 2B, the equilibrium dissociation constant (K_D) value of Lathyrol was $20.90 \pm 2.34 \mu\text{M}$, displaying a strong binding affinity to MAFF. In the CETSA assay, Lathyrol increased the cellular thermal stability of MAFF protein from a tolerated temperature of 70 to 72 °C (Figure 2C). In the DARTS assay, about 50% of the MAFF protein in cell lysates was degraded within 15 min after being treated with pronase, whereas the degradation of MAFF was significantly reduced after Lathyrol treatment (Figure 2D). Based on the results listed above, MAFF can be confirmed to be a direct target of Lathyrol. Besides, to intuitively observe the co-localization of Lathyrol and MAFF protein in RAW264.7 cells, we synthesized a fluorescent probe (naphthalimide-conjugated Lathyrol), named ZCY-probe (Figure 2E), as described in Scheme S1 of Supporting Information. The result showed that MAFF protein was located in the nucleus as expected and Lathyrol was mainly co-located in the nucleus in cells treated with the ZCY-probe (Figure 2F), indicating the direct interaction between Lathyrol and MAFF in cells.

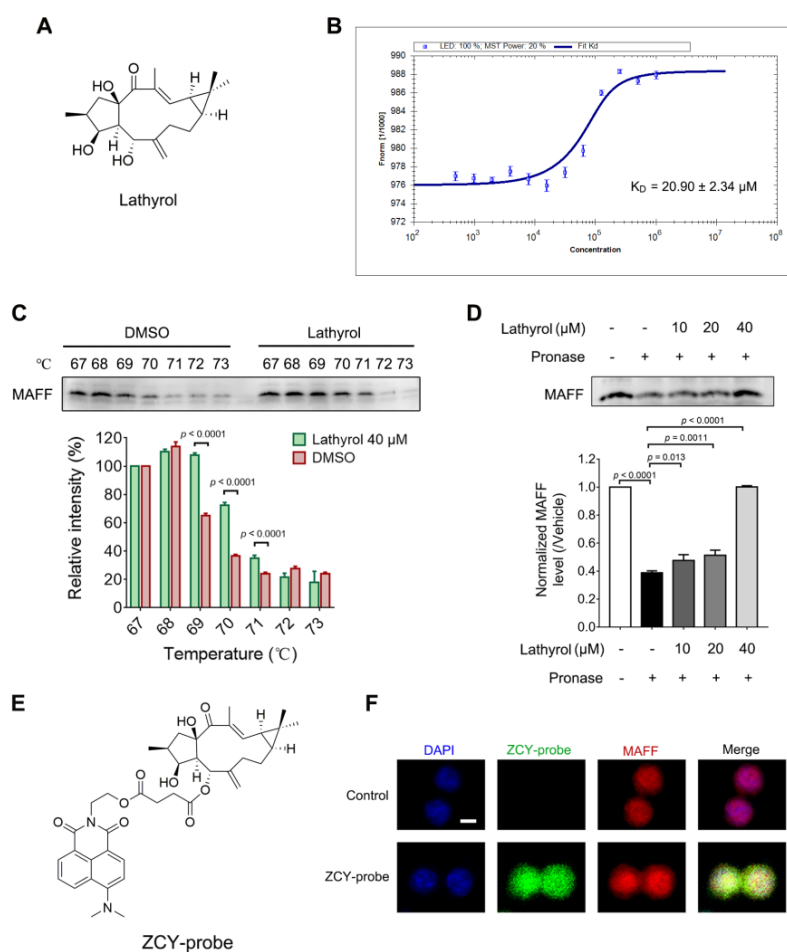


Figure 2. Lathyrol directly binds to MAFF. (A) Structure of Lathyrol. **(B)** MST assay to measure the binding affinity between Lathyrol and MAFF protein. $n = 3$. Data are presented as mean \pm SD. **(C)** CETSA assay to detect the thermal stability of cellular MAFF protein. **(D)** DARTS assay to test the stability of cellular MAFF protein under enzyme degradation. **(E)** Structure of the fluorescent ZCY-probe. **(F)** Representative immunofluorescence images of intracellular distribution of ZCY-probe (green) and MAFF (red) in RAW264.7 cells pretreated for 8 h with ZCY-probe (10 μ M) or DMSO. Nuclei were labeled with DAPI (blue). Scale bars, 5 μ m.

MAFF is the target of ZCY020

After proving MAFF to be a direct target of Lathyrol, ZCY020, a lathyrane diterpenoid isolated from *Euphorbia lathyris* (Figure 3A) also undergone assays to assess its ability to bind with MAFF. Encouragingly, ZCY020 presented a relatively stronger binding affinity to MAFF than Lathyrol, and the K_D value in MST assay was $19.50 \pm 1.70 \mu$ M (Figure 3B). Further, the CETSA assay and DARTS assay were confirmed that MAFF was also a direct target of ZCY020 (Figure 3C-3D). Considering the strong NO inhibitory activity, same core scaffold structure, and large amount of ZCY020 in the seeds of *Euphorbia lathyris*, it was used as a representative lathyrane diterpenoid for further studying the anti-inflammatory activity and mechanism *in vitro* and *in vivo*.

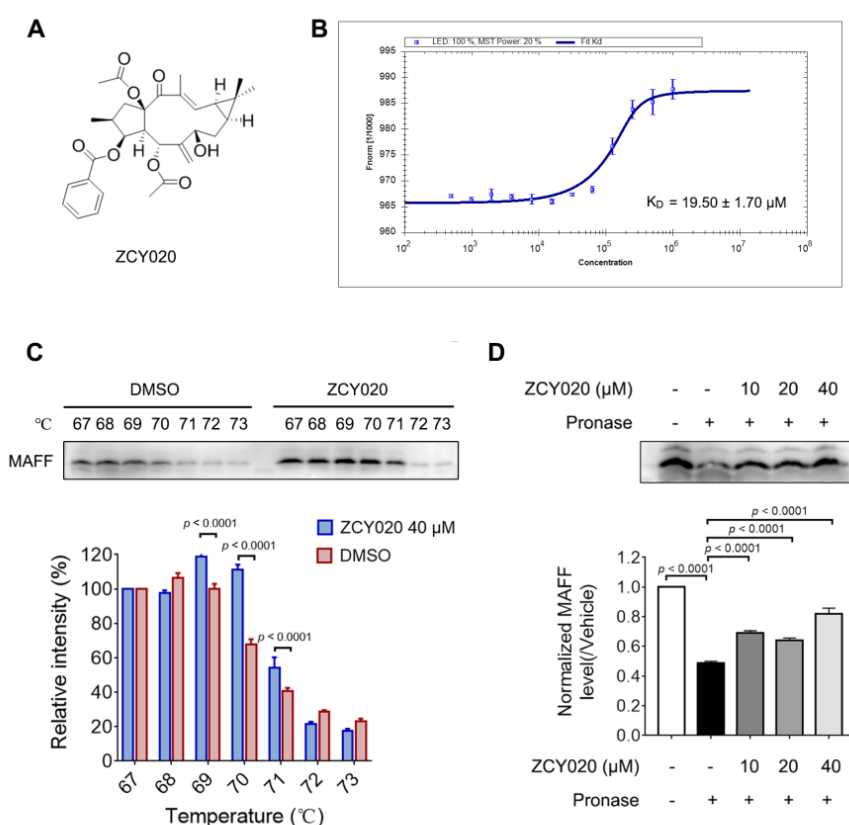


Figure 3. MAFF is the target of ZCY020. (A) Structure of ZCY020. **(B)** MST assay to measure the binding affinity between ZCY020 and MAFF protein. $n = 3$. Data are presented as mean \pm SD. **(C)** CETSA assay to detect the thermal stability of cellular MAFF protein. **(D)** DARTS assay to test the stability of cellular MAFF protein under enzyme degradation.

ZCY020 inhibits the formation of MAFF homodimer and promotes the heterodimerization of MAFF and Nrf2

It has been reported that transcriptional regulation through the MARE element relies on a delicate and sensitive balance between the activated CNC molecules and their small Maf partners. Overexpression of sMafs inhibits MARE-dependent transcription by competitively binding to the DNA region with CNC transcription factors including nuclear factor-erythroid 2-p45-related factor 2 (Nrf2) [27]. Nrf2 is a master regulator of antioxidative and anti-inflammatory genes through the heterodimers with the small Maf proteins [23]. Under normal stress-free conditions, Nrf2 is ubiquitinated by keap1-E3 ubiquitin ligase complex and degraded by proteasome system [33]. However, when induced by oxidative stress or inflammatory mediators, Nrf2 is released from Keap1, translocates into the nucleus, forms heterodimer with sMAFs, and transactivates the expression of several antioxidant and anti-inflammatory genes [34].

As expected, upon LPS stress, MAFF expression in nucleus increased, while Nrf2 slightly increased and was mainly transferred into the nucleus before forming heterodimers with MAFF (Figure 4A). After treatment with ZCY020, the nuclear translocation of Nrf2 became more significant, and the formation of the heterodimer of MAFF-Nrf2 also increased in a dose-dependent manner (Figure 4A). The transcriptional repression by sMAFs homodimer requires sumoylation and is specifically modified by SUMO-2/3 [35]. Thus, the sumoylation level of MAFF was evaluated by co-immunoprecipitation (CO-IP) experiments. It was shown that LPS stimuli obviously elevated the sumoylation of MAFF and its binding with SUMO-2/3, while ZCY020 significantly suppressed these effects (Figure 4B).

Since ZCY020 promoted the formation of heterodimer of MAFF and Nrf2 and inhibited MAFF homodimerization in LPS-induced RAW264.7 cells, we then sought to investigate whether ZCY020 represses the formation of MAFF homodimers with itself or other sMAFs, and whether it promotes MAFF to bind with Nrf2 in basal RAW264.7 cells and HEK293T cells. CO-IP analysis confirmed that ZCY020 inhibited the binding of MAFF both to itself and to MAFK, but enhanced the interaction of MAFF with Nrf2 (Figure 4C-4E). These studies revealed a previously unproved mechanism, suggesting that ZCY020 mediates the positive transcription of MAFF-Nrf2 regulatory genes via inhibiting MAFF homodimers and boosting the formation of MAFF-Nrf2 heterodimer.

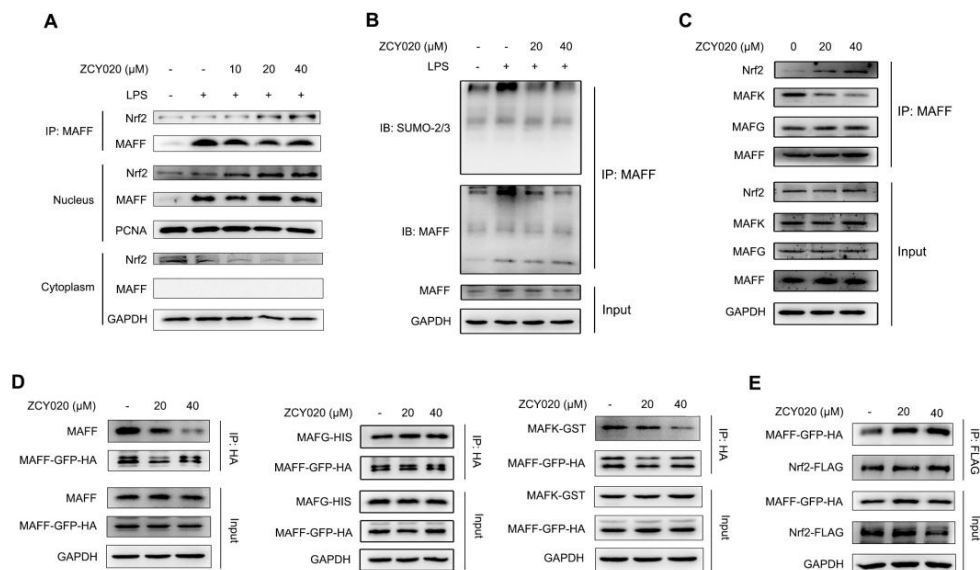


Figure 4. ZCY020 inhibits the formation of MAFF homodimer and promotes the heterodimerization of MAFF and Nrf2. (A) Immunoprecipitation assay of MAFF and Nrf2 in LPS-induced RAW264.7 cells treated with ZCY020 (0, 10, 20 and 40 μ M, respectively). (B) Immunoprecipitation assay of MAFF and SUMO-2/3 in LPS-induced RAW264.7 cells treated with ZCY020 (40 μ M). (C) Immunoprecipitation assay in basal RAW264.7 cells treated with ZCY020 (20 and 40 μ M). (D) Immunoprecipitation assays in HEK293T cells transfected with GFP-HA-tagged MAFF (MAFF-GFP-HA) alone or MAFF-GFP-HA and HIS-tagged MAFK (MAFG-HIS) or MAFF-GFP-HA and GST-tagged MAFK (MAFK-GST). (E) Immunoprecipitation assay in HEK293T cells transfected with GFP-HA-tagged MAFF (MAFF-GFP-HA) and FLAG-tagged Nrf2 (Nrf2-FLAG). FLAG antibody was used to immunoprecipitate Nrf2-FLAG and MAFF-GFP-HA.

ZCY020 activates MAFF-Nrf2/HO-1 pathway

Nrf2 forms heterodimers with sMAFs in nucleus, positively activating the transcription of target genes including heme oxygenase 1 (*HMOX1*), NADPH quinone dehydrogenase 1 (*NQO1*), glutamate-cysteine ligase catalytic subunit (*GCLC*) and modifier subunit (*GCLM*), constituting the main cytoprotective defense system in cells [36]. LPS mildly increased the gene expression of *HMOX1*, *NQO1* and *GCLM*, a proper adaptive response to oxidative stress [37], which was potentiated by ZCY020; besides, the impaired gene expression of *GCLC* was also restored by ZCY020 (Figure 5A). HMOX1 (HO-1), one of the classic Nrf2-regulated proteins, is induced in response to stimulus such as hypoxia, oxidative stress, cytokines, LPS, heavy metals in biological systems, and a tremendous amount of works have demonstrated that HO-1 have significant antioxidant and anti-inflammatory effects mediated by Nrf2 [38-44]. Thus, activation of the Nrf2/HO-1 axis through MAFF-Nrf2 heterodimer can be beneficial to anti-inflammatory effects.

Not surprisingly, ZCY020 significantly up-regulated the level of Nrf2 protein, and attenuated the overexpression of MAFF protein induced by LPS. Meanwhile, consistent with the level of Nrf2, HO-1 protein expression also increased dose-dependently (Figure 5B). Keap1 is an inhibitor of Nrf2 transcription activity through ubiquitination and proteasome degradation under basal conditions [33]. Consistently, LPS induced the decreased expression of Keap1 in RAW264.7 cells, which were further promoted by ZCY020 treatment (Figure 5B). The increased nuclear translocation of Nrf2 was also further confirmed by immunofluorescence assay (Figure 5C). Therefore, the antioxidant activity of ZCY020 was then detected in LPS-induced RAW264.7 cells. Reactive oxygen species (ROS) are key signaling molecules that play an important role in the progression of inflammatory disorders [45]. ZCY020 treatment dose-dependently inhibited the production of ROS stimulated by LPS (Figure 5D).

To verify that ZCY020 activates Nrf2 pathway through MAFF-Nrf2 heterodimer, an Nrf2 inhibitor ML385 was used to interfere with the binding of the sMAFs-NRF2 protein complex [46]. The HO-1 expression was significantly decreased in cells pretreated with ML385 compared with only ZCY020 treated controls (Figure 5E). Meanwhile, ML385 reversed the expression and nuclear translocation of Nrf2, and the inhibition effect on ROS by ZCY020 stimulation (Figure 5F and 5G). These results were further validated by HO-1 expression and ROS levels in MAFF-silenced RAW264.7 cells (Figure 5H) after ZCY020 treatment, which exhibited decreased HO-1 expression and increased ROS levels in shMAFF cells (Figure 5I and 5J). Thus, the above studies indicate that ZCY020 activates the Nrf2/HO-1 pathway to exert antioxidant effects through MAFF-Nrf2 heterodimers.

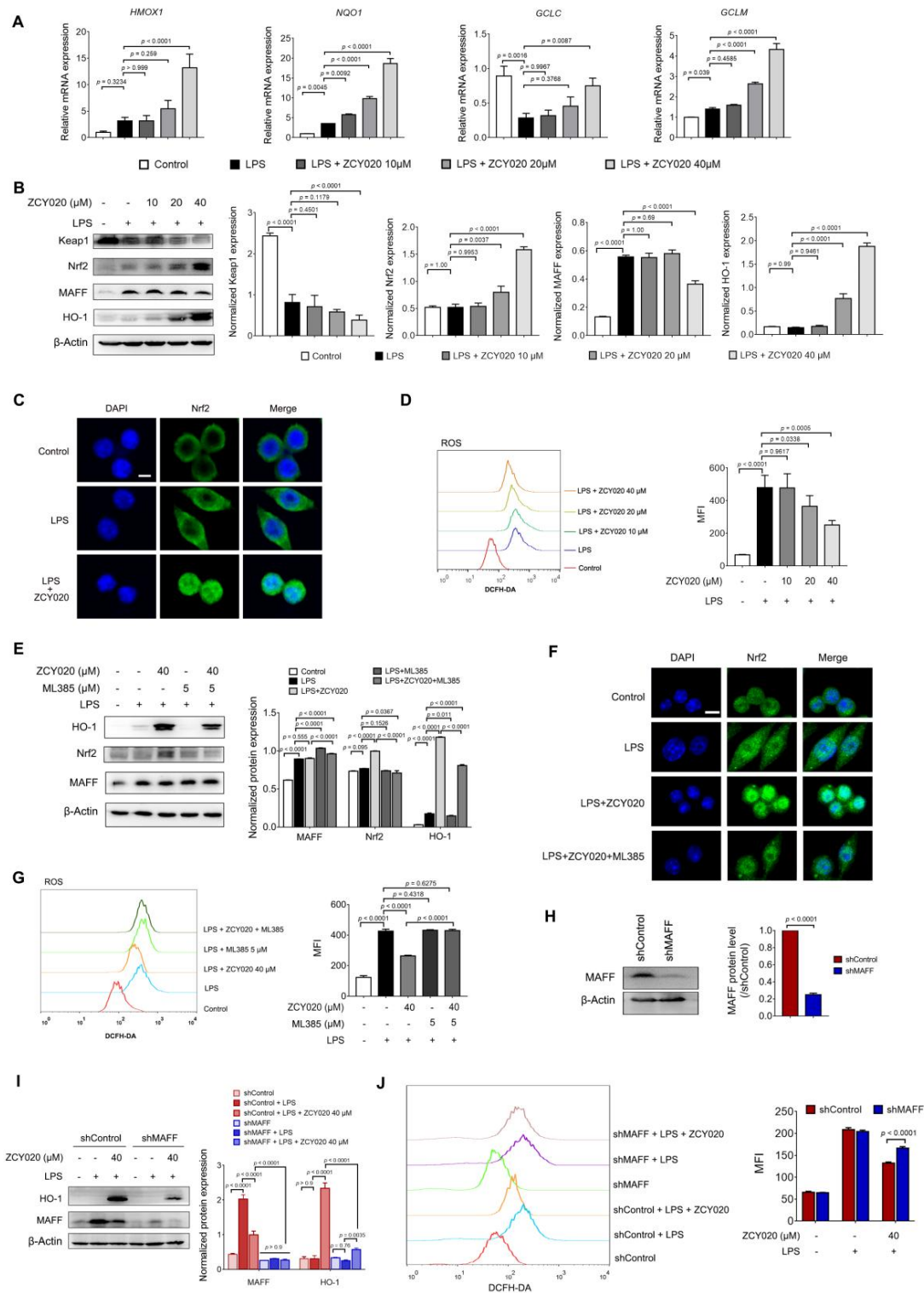


Figure 5. ZCY020 activates MAFF-Nrf2 pathway. (A) Gene expressions of *HMOX1*, *NQO1*, *GCLC* and *GCLM* were detected by RT-qPCR. $n = 3$. Data are presented as mean \pm SD. Each gene was normalized to β -Actin gene (*ACTB*). (B) Immunoblot analysis of protein expressions of MAFF, Nrf2, Keap1 and HO-1. (C) Immunofluorescence analysis of Nrf2 (green) in LPS-induced RAW264.7 cells. Nuclei were labeled with DAPI (blue). (Scale bar: 20 μ m.) (D) Flow cytometry analysis of reactive oxygen species (ROS) levels in LPS-induced RAW264.7 cells. (E) Expression levels of MAFF, Nrf2

and HO-1 in RAW264.7 cells after 40 μM ZCY020 alone or in combination with 5 μM ML385 treatments. **(F)** Immunofluorescence analysis of Nrf2 (green) in LPS-induced RAW264.7 cells after 40 μM ZCY020 alone or in combination with 5 μM ML385 treatments. Nuclei were labeled with DAPI (blue). Scale bar: 20 μm . **(G)** ROS levels in RAW264.7 cells after 40 μM ZCY020 alone or in combination with 5 μM ML385 treatments. **(H)** Expression levels of MAFF in shControl and shMAFF RAW264.7 cells. **(I)** Immunoblot analysis of HO-1 and MAFF expressions in shControl and shMAFF cells after ZCY020 treatment. **(J)** ROS levels in shControl and shMAFF cells after ZCY020 treatment. Immunoblot analysis data were normalized with β -Actin.

ZCY020 inhibits LPS-induced inflammatory responses

Nrf2 has been proved to dampen the inflammatory responses triggered by LPS, and HO-1 is at the core of Nrf2-mediated inhibition of the NF- κ B pathway [39,47-49], which plays a major role in the development of inflammation [50]. Since ZCY020 was proved to promote Nrf2 activation and HO-1 expression, we further explored the anti-inflammatory activity of ZCY020 in LPS-induced RAW264.7 cells. Notably, ZCY020 inhibited the phosphorylation of I κ B α and the nuclear translocation of NF- κ B p65 (Figure 6A and 6B), two key steps in the activation of NF- κ B pathway [50]. Besides, the expression levels of inducible nitric oxide synthase (iNOS) and cyclooxygenase-2 (COX-2) were up-regulated after LPS treatment, which were then reduced by treatment with ZCY020 dose-dependently (figure 6C). And ZCY020 strongly inhibited NO production with an IC₅₀ value of $6.36 \pm 0.55 \mu\text{M}$ (Figure 6D).

Thus, the transcriptional levels and protein release levels of pro-inflammatory cytokines interleukin (IL)-1 β , IL-6 and tumor necrosis factor (TNF)- α were measured. As expected, ZCY020 significantly decreased the transcription and expression of IL-1 β , IL-6 and TNF- α in a dose-dependent manner (Figure 6E and 6F). Furthermore, MAFF silencing using shRNA weakened the inhibitory effect of ZCY020 on the phosphorylation of I κ B α and NO release induced by LPS, with the IC₅₀ value increasing to $15.21 \pm 0.78 \mu\text{M}$ (Figure 6G and 6H). Taking these results together, it can be verified that ZCY020 suppresses the activation of the NF- κ B pathway through targeting MAFF.

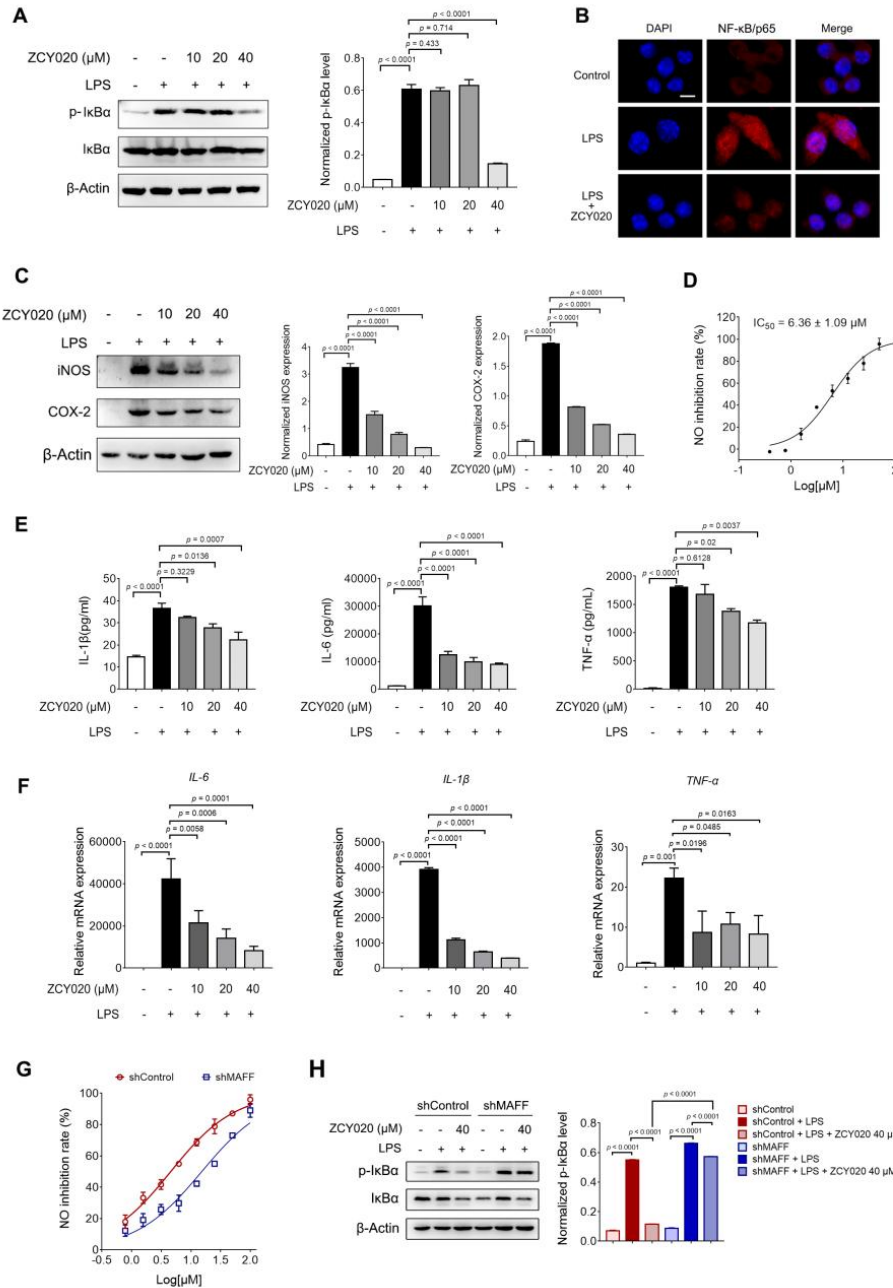


Figure 6. ZCY020 inhibits NF-κB signaling pathway. (A) Immunoblot analysis of IκBα and p-IκBα. **(B)** Immunofluorescence analysis of NF-κB (red) in LPS-induced RAW264.7 cells. Nuclei were labeled with DAPI (blue). Scale bar, 20 μm. **(C)** Immunoblot analysis of protein expression of iNOS and COX-2. **(D)** Inhibition of NO production by ZCY020. *n* = 3. Data are presented as mean ± SD. **(E)** Cytokine levels of IL-1β, IL-6 and TNF-α in LPS-induced RAW264.7 cell medium after exposure to ZCY020. *n* = 3. Data are presented as mean ± SD. **(F)** Gene expressions of *IL-6*, *IL-1β* and *TNF-α* were detected by RT-qPCR. *n* = 3. Data are presented as mean ± SD. Each gene was normalized to β-Actin gene (*ACTB*). **(G)** Inhibition of NO production in shControl and shMAFF cells after ZCY020 treatment. *n* = 3. Data are presented as mean ± SD. **(H)** Immunoblot analysis of IκBα and p-IκBα in shControl and shMAFF cells after ZCY020 treatment. Immunoblot analysis data were normalized with β-Actin.

ZCY020 promotes the maintenance of mitochondria quality control

The mitochondria play a central role in bioenergetics and respiratory functions for cell viability through numerous biochemical processes. Oxidative stress by ROS triggers mitochondrial dysfunction; meanwhile, mitochondrial damage directly promotes the increase of mitochondrial ROS (mtROS) production [51]. The production of excess mtROS further promotes the secretion of inflammatory cytokines and immune cell activation [52]. Therefore, eliminating excess mtROS and the amount of damaged mitochondria is a key challenge to the inhibition of inflammation. Mitophagy is a selective form of autophagy, which can remove dysfunctional mitochondria to maintain the overall health of mitochondria [53]. Vast studies have indicated that Nrf2 activation prevents mitochondrial excessive fission and further synthesis of mtROS, while promoting mitophagy and maintaining mitochondria quality control [54-56].

Herein, we suspected that ZCY020 could reduce excess mtROS and promote mitophagy through the MAFF-Nrf2 pathway. We first investigated mitochondrial superoxide production at 12 h after LPS challenge in macrophages using a mitochondrial superoxide indicator MitoSOX. As shown in [Figure 7A](#), LPS evidently increased the production of mitochondrial superoxide, which was dose-dependently reversed by ZCY020 pretreatment. Furthermore, the effect of ZCY020 on mitophagy activation in LPS-induced cells was then explored. Sequestosome 1 (SQSTM1)/p62, a crucial autophagic adaptor protein involved in mitophagy, is important for the maintenance of mitochondrial integrity and energy production [57,58]. Followed by the up-regulation of Nrf2, an increased expression of p62 was observed after administration with ZCY020 ([Figure 7B](#)). BNIP3 (BCL2 interacting protein 3), a major mitophagy receptor on the outer mitochondrial membrane, can interact with the microtubule-associated protein 1 light chain 3 (LC3) and then target the autophagy machinery to mitochondria [59]. As expected, ZCY020 significantly promoted the expression of BNIP3 and the abundance of LC3B-II after LPS stimulation ([Figure 7C](#)). These results reveal that ZCY020 decreases LPS-induced mtROS production and facilitates mitophagy to maintain mitochondria homeostasis.

We then validated the effects of ZCY020 on mitochondria homeostasis using ROS scavenger N-acetylcysteine (NAC). NAC has been reported to inhibit ROS production and autophagy [60,61]. Compared with ZCY020 treatment, pre-treatment with NAC significantly attenuated the increase of p62, BNIP3 and LC3B-II ([Figure 7D](#)). LC3B/BNIP3 dot formation was also performed by immunofluorescence assay to detect autophagosomes in RAW264.7 cells. The results showed that ZCY020 treatment increased LC3B and BNIP3 expression and co-location in cells, and accelerated autophagosome accumulation which was reversed by pre-treatment with NAC ([Figure 7E](#)). Therefore, these studies demonstrate that ZCY020 promotes mitophagy. To confirm that ZCY020 exerts such effects through the MAFF-Nrf2 pathway, the Nrf2 inhibitor ML385 was applied. As shown in the results, the inhibitory effects on mitochondrial superoxide ([Figure 7F](#)) and the facilitating effects on BNIP3 and LC3B-II ([Figure 7G](#)) of ZCY020 were blocked by ML385. Furthermore, MAFF shRNA hindered the up-regulation of ZCY020 on the expression p62, BNIP3 and LC3B-II ([Figure 7H](#)). These results suggest that ZCY020 inhibits LPS-induced mtROS production and boosts mitophagy via MAFF-Nrf2 pathway by targeting MAFF.

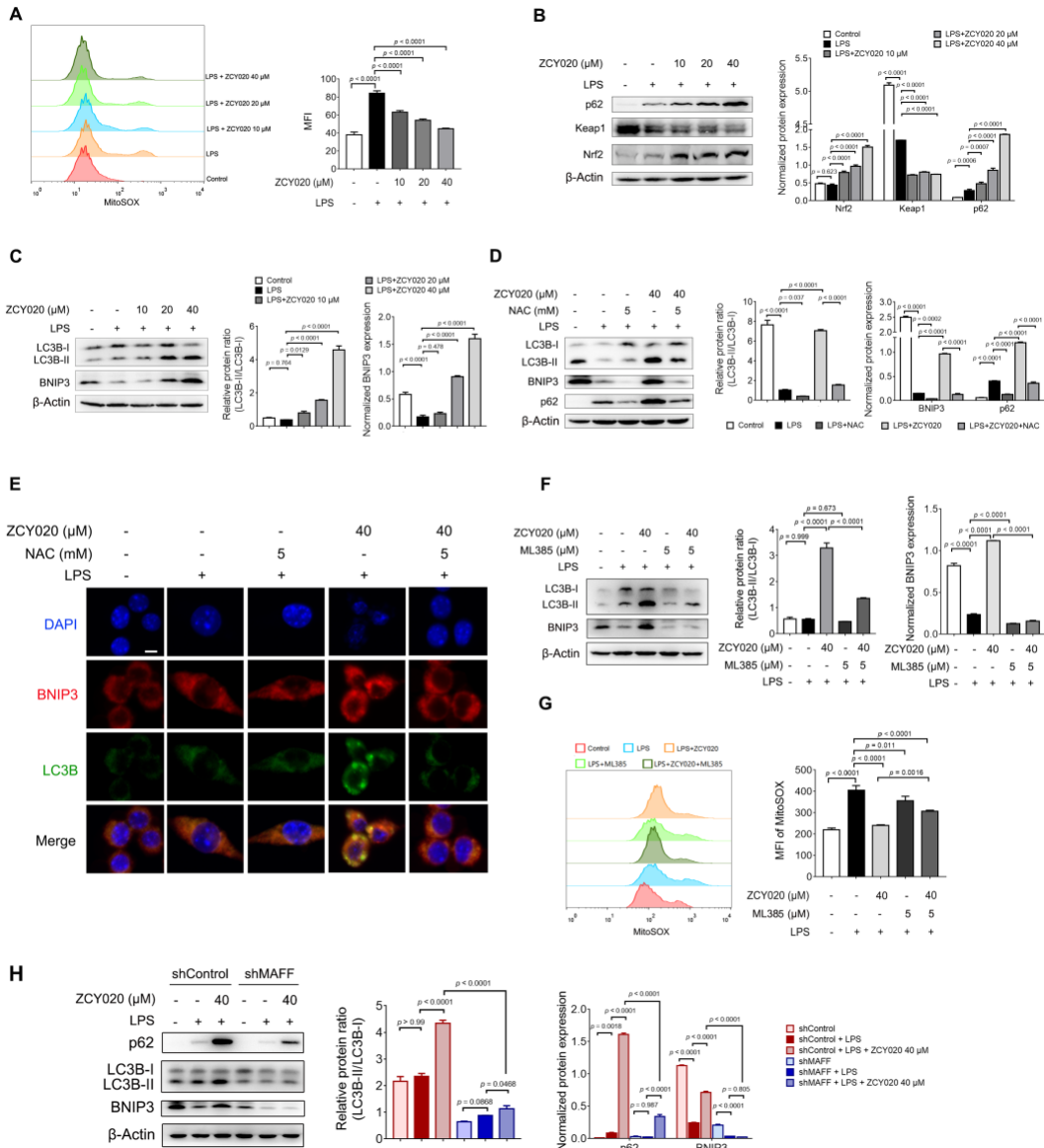


Figure 7. ZCY020 promotes the maintenance of mitochondria quality control. (A) Flow cytometry analysis of mitochondrial superoxide (mitoSOX) levels in LPS-induced RAW264.7 cells. (B) Immunoblot analysis of protein expression of p62, Keap1 and Nrf2 in LPS-induced RAW264.7 cells. (C) Immunoblot analysis of protein expression of LC3B and BNIP3. (D) Expression levels of LC3B, BNIP3 and p62 in LPS-induced RAW264.7 cells after 40 μM ZCY020 alone or in combination with 5 mM NAC treatments. (E) Immunofluorescence analysis of LC3B (green) and BNIP3 (red) in LPS-induced RAW264.7 cells treated with 40 μM ZCY020 alone or in combination with 5 mM NAC. Nuclei were labeled with DAPI (blue). (Scale bar: 20 μm.) (F) Expression levels of LC3B and BNIP3 in LPS-induced RAW264.7 cells after 40 μM ZCY020 alone or in combination with 5 μM ML385 treatments. (G) The levels of mitoSOX in LPS-induced cells pretreated with 40 μM ZCY020 alone or in combination with 5 μM ML385. (H) Immunoblot analysis of p62, BNIP3 and LC3B in shControl and shMAFF cells after ZCY020 treatment. Immunoblot analysis data were normalized with β-Actin.

ZCY020 shows inhibitory effects on LPS-induced acute lung injury in mice.

To further evaluate the anti-inflammation of ZCY020 *in vivo*, we next assessed the *in vivo* anti-inflammatory effects of ZCY020 on LPS-stimulated acute lung injury (ALI) in mice. LPS, a major cell wall component of Gram-negative bacteria, can serve as an endotoxin to cause a systemic inflammatory response, acute tissue injury and even death in mice [62]. Oral administration of ZCY020 effectively inhibited the LPS-caused mortality in a pleasant dose-dependent manner. All 10 mice died within 24 h in the 15 mg/kg LPS exposure group, but after ZCY020 administration, at day 8, the survival rate of mice in the low dose (50 mg/kg) group was 20%, and in the high dose (100 mg/kg) group, the survival rate was even up to 60% (Figure 8A). Histopathological analysis showed that in the lungs of LPS-treated mice, serious inflammatory cell infiltration and obvious thickening of alveolar wall occurred, which were effectively inhibited by ZCY020 administration (Figure 8B). Meanwhile, ZCY020 treatment effectively protected the livers of mice against LPS-caused inflammatory cell infiltration and hepatocyte damage (Figure 8B). Moreover, inflammatory cytokines IL-1 β , IL-6 and TNF α in the blood were significantly reduced dose-dependently by ZCY020 in mice injured by LPS (1.5 mg/kg) (Figure 8C). These results suggest that ZCY020 can significantly inhibit inflammatory responses and reduce subsequent tissue and organ injuries with high efficacy.

The transcription levels of *IL-1 β* , *IL-6* and *TNF- α* were also detected in mouse lung tissues and significantly decreased after ZCY020 treatment (Figure 8D). The change of MAFF-Nrf2 pathway in mouse lung tissues induced by ZCY020 treatment was also evaluated. As expected, the transcription levels of *HMOX1*, *NQO1*, *GCLC* and *GCLM* were up-regulated by ZCY020 (Figure 8E). Besides, ZCY020 administration increased the expression of Nrf2, and promoted the transcription and expression of HO-1 in the lung tissues (Figure 8F). Notably, in response to the stress of high dose of LPS, ZCY020 markedly increased the expression of MAFF (Figure 8F). Moreover, the expression of BNIP3 and the abundance of LC3B-II in mouse lung tissues were elevated significantly by ZCY020, although LC3B-I was also sharply up-regulated (Figure 8G). The phosphorylation level of I κ B α dropped after ZCY020 treatment (Figure 8H), indicating the inhibition of NF- κ B activation. Together, these results provide evidence that ZCY020 transcriptionally activates the MAFF-Nrf2 pathway, promotes mitophagy, and inhibits NF- κ B activation, exerting anti-oxidant and anti-inflammatory effects against ALI.

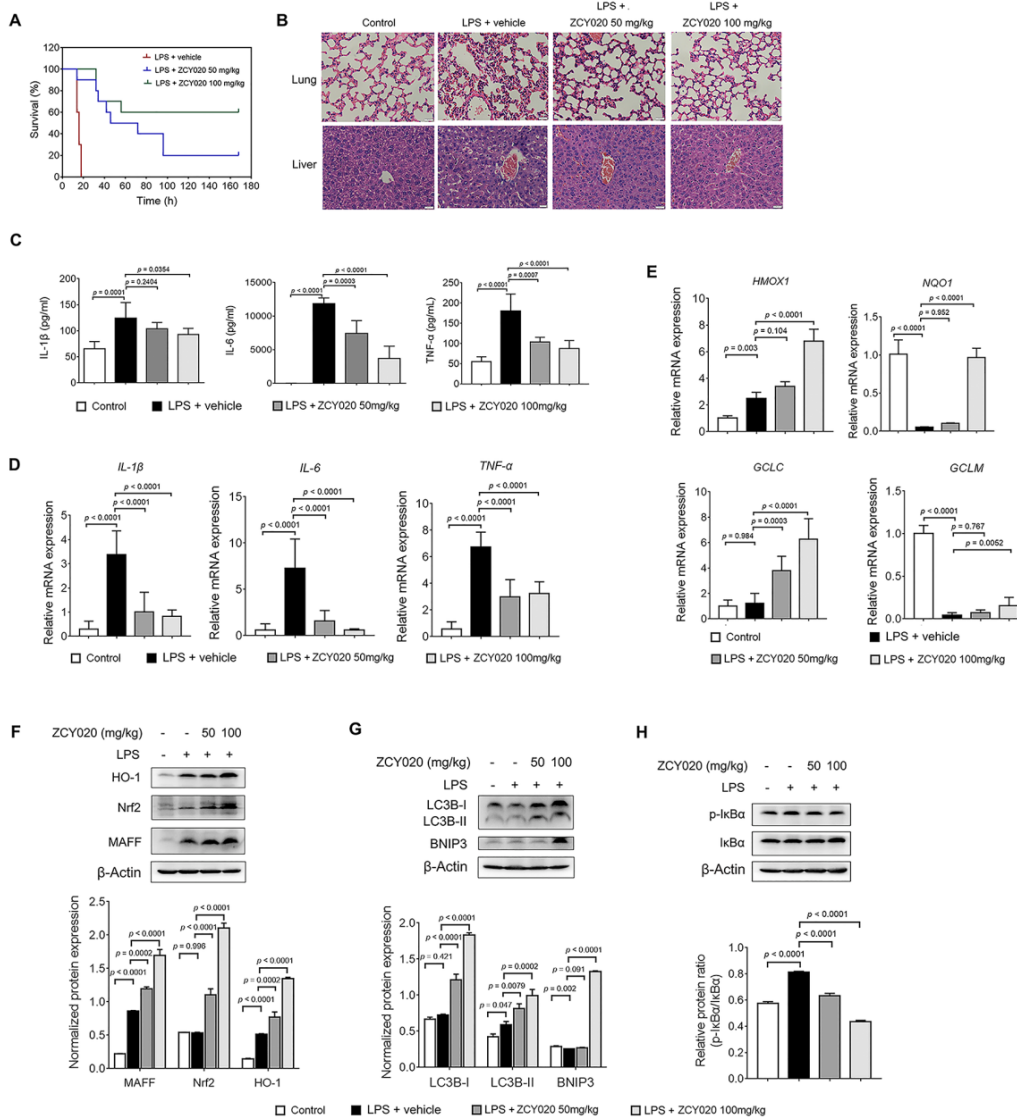


Figure 8. ZCY020 shows inhibitory effects on LPS-induced acute lung injury in mice. (A) Survival rate of mice during one week after LPS and/or ZCY020 exposure. BALB/C mice were orally treated with ZCY020 or vehicle at 2 h before injection of 15 mg/kg LPS and at 12, 24, 48, 72 and 96 h after the injection of LPS. Survival rate was monitored daily. $n = 10$ per group. **(B)** Representative H&E stained sections prepared from lung and liver tissues, magnification 400 \times . **(C)** Inflammatory cytokines IL- β and IL-6 in the blood were measured at 4 h after LPS challenge by ELISA. BALB/C mice were orally treated with ZCY020 or vehicle 90 min before 1.5 mg/kg LPS injection. Four hours later, the serum was collected for ELISA. $n = 6$ per group. Data are presented as mean \pm SD. **(D)** Gene expression of *IL-1 β* , *IL-6* and *TNF- α* detected by RT-qPCR. $n = 3$. Data are presented as mean \pm SD. Each gene was normalized to β -Actin gene (*ACTB*). **(E)** Gene expression of *HMOX1*, *NQO1*, *GCLC* and *GCLM* detected by RT-qPCR. $n = 3$. Data are presented as mean \pm SD. Each gene was normalized to β -Actin gene (*ACTB*). **(F)** Immunoblot analysis of protein expression of HO-1, Nrf2 and MAFF in mouse lung tissues. **(G)** Immunoblot analysis of protein expression of LC3B and BNIP3. **(H)** Immunoblot analysis of the phosphorylation level of I κ B α . Immunoblot analysis data were normalized with β -Actin.

DISCUSSION

Target identification is of great significance for the development of new drugs and the elaboration of their pharmacological effects, especially for natural products with unknown mechanisms of action. Basically, target identification strategies include three approaches: affinity-based target identification, activity-based protein profiling (ABPP), and label-free target identification [63]. ABPP is designed specifically for the identification of functionally active proteins, such as enzymes [64,65]. Conventional affinity-based pull-down approaches depends on the transient binding events between bioactive small molecules and target proteins, and this binding is required to be strong enough to allow the isolation of target proteins from the whole proteome [66]. Besides, the accuracy of the pull-down assay is significantly affected by the experimental design and operation. Existing label-free target identification methods, such as DARTS or CETSA-combined mass spectrometry, are also limited by target binding affinity and target proteins' susceptibility to proteolysis or thermal denaturation [67,68].

In this study, we proposed a novel approach for identifying the possible targets of natural products via PROTAC technology. We synthesized a PROTAC (ZCY-PROTAC) derived from Lathyrol and CRBN ligand thalidomide, and verified the MAFF protein as a potential target of Lathyrol by comparative quantitative proteomics in which the decreased expression levels of potential targets was induced by the degrader. Using biochemical and pharmacological approaches, we further validated that Lathyrol and ZCY020 directly binds with MAFF, and that ZCY020 exerts antioxidative and anti-inflammatory effects through MAFF-Nrf2 pathway *in vitro* and *in vivo*. This study demonstrates the feasibility and reliability of PROTAC technique to identify the potential targets of natural products.

Unlike affinity-based target identification, target identification by PROTAC method do not always require strong binding between targets and the compound, but only depend on the formation of the target-PROTAC-E3 ligase ternary complex [69,70]. As long as the degradation of targets is observed, the method can be seen as durable. Also, when assessing natural products, which tend to have multiple targets and only moderate binding affinities with their target, affinity-based target identification methods have a higher chance to get false-positive and false-negative results. Therefore PROTAC-based target identification will be an excellent alternative for currently available approaches. Furthermore, the readout of PROTAC based target identification is the final degradation results from comparative quantitative proteomics, which is an amplified signal to some extent. And with the omission of the pull-down assay required in affinity-based methods, PROTAC-based target identification may eradicate the error caused by experimental design and operation.

In this study, PROTAC treatment followed by quantitative proteomic analysis was applied to identify MAFF protein as the potential target of Lathyrol. As mentioned above, the direct binding of MAFF with Lathyrol was further verified by MST, CETSA and DARTS assays. ZCY020, a Lathyrol derivative with abundant amount and considerable activity, was chosen for further mechanism studies both *in vitro* and *in vivo*. Consistent with previous studies [28-30], our data suggested that LPS markedly increases MAFF expression, whereas ZCY020 reverses this effect and keeps it at a certain level. At the same time, the expression and the level of nuclear translocation of Nrf2 were increased by ZCY020, and these changes went on to facilitate the formation of the MAFF-Nrf2 heterodimer. The immunoprecipitation assay result confirmed the viewpoint that ZCY020 promoted the interaction between MAFF and Nrf2 in both LPS-injured RAW264.7 cells and

transfected HEK293T cells, and thus promoted Nrf2-regulated antioxidant and anti-inflammatory response.

Nrf2 and its regulated protein HO-1 have been reported to be important regulators in inflammation, and the Nrf2/HO-1 axis plays a major role in antioxidant and anti-inflammatory function [38,39]. Our studies indicated that in LPS-simulated macrophages, ZCY020 distinctly promoted the transcription and expression of HO-1 through promoting formations of MAFF-Nrf2 heterodimer, thus inhibiting the production of ROS and the activation of NF- κ B pathway. In addition, Nrf2 has been reported to be positively associated with mitochondrial biogenesis and mitochondrial quality control [55,56], which are also powerful means employed by mitophagy to keep the immune system in check [56,71]. Our results were consistent with this statement and showed that ZCY020 promoted mitochondrial quality control through two aspects: eliminating mtROS and accelerating mitophagy. Notably, p62 was significantly up-regulated when mitophagy was boosted by ZCY020, which is consistent with other studies [72,73] that p62 promotes the release and nuclear translocation of Nrf2 by mediating the degradation of Keap1 through selective autophagy, and Nrf2 also up-regulates the expression of p62, creating a p62-Keap1-Nrf2 positive feedback loop that further enhances the protective effect.

Since ZCY020 showed effective anti-inflammatory activity *in vitro*, we continued to study its effect *in vivo*. Acute lung injury (ALI) and acute respiratory distress syndrome (ARDS) are severe clinical symptoms in intensive care units with high morbidity and mortality in critically ill patients, including in SRAS, MERS and COVID-19 [74, 75]. When the immune system is over-activated due to viral or bacterial infection, a large number of pro-inflammatory cytokines may be secreted, leading to the formation of a cytokine storm and causing rapid single organ or multiple organ failure and ultimately threatening life [76, 77]. In this study, when injected with LPS, the release of pro-inflammatory cytokines in mice increased significantly, and inflammatory cell infiltration and damage appeared in the lungs and liver, and even death occurred. ZCY020 effectively reversed these symptoms of ALI and reduced mice mortality in a dose-dependent manner. Further investigations demonstrated that ZCY020 elevated the expression of Nrf2 and the target regulated protein HO-1, inhibiting the activation of NF- κ B, and promoting mitophagy. These results were in keeping with our findings *in vitro*.

In summary, we creatively employed PROTAC technology to explore the targets of natural products, by using the degrader as the probe, combined with quantitative proteomics to observe the changes of proteome before and after, then confirmed that MAFF is a key target protein of lathyrane diterpenoids. Based on this evidence, we verified that lathyrane diterpenoid ZCY020 exerts anti-inflammatory effects by decreasing ROS production, inhibiting NF- κ B activation, and maintaining mitochondrial quality through the MAFF-Nrf2 pathway in LPS-induced RAW264.7 macrophages and ALI mice. These results suggest that the method of protac probes combined with quantitative proteomics, which we call Targeted Degradomics here, can be a novel and valuable supplementary approach for the target identification of natural products and other drugs, and is worthy of further application and investigation.

MATERIALS AND METHODS

General Chemistry Methods

All commercially available starting materials and solvents were reagent grade and used

without further purification. Reactions were monitored by thin-layer chromatography (TLC) on 0.25 mm silica gel plates (GF₂₅₄) and visualized under UV light or by heating after spraying with anisaldehyde-H₂SO₄ reagent. ¹H NMR and ¹³C NMR spectra were recorded on a Bruker AV-600 spectrometer (Bruker Biospin, Fallanden, Switzerland). Chemical shifts are stated relative to TMS and expressed in δ values (ppm), with coupling constants reported in Hz. High resolution mass spectra (HR-MS) of all derivatives were recorded on a Bruker solarix or micrOTOF focusII mass spectrometry by electrospray ionization (ESI). All tested compounds had a purity of >95%. Detailed synthetic procedure of ZCY-probe and spectral characterization for all compounds are provided in the [Supporting Information](#).

General procedure to synthesize ZCY-PROTAC

Synthesis of Lathyrol

Euphorbia factor L3 (5 g) in 5% KOH/MeOH (100 mL) was stirred at room temperature for 6-8 h. Upon completion, the solvent was removed under reduced pressure, and the residue was extracted with DCM, washed with brine, dried with anhydrous Na₂SO₄, filtered, evaporated and purified by silica gel column chromatography (CC) to afford lathyrol as white solid (82% yield). ¹H NMR (600 MHz, CDCl₃) δ 5.98 (dd, J = 10.5, 1.1 Hz, 1H), 5.04 (t, J = 1.4 Hz, 1H), 4.90 (s, 1H), 4.46 (s, 1H), 4.38 (s, 1H), 4.30 (q, J = 3.4 Hz, 1H), 3.41 (d, J = 3.6 Hz, 1H), 3.32 (d, J = 3.8 Hz, 1H), 2.73 (dd, J = 14.8, 9.8 Hz, 1H), 2.46 (dd, J = 14.1, 7.9 Hz, 1H), 2.20 (t, J = 3.5 Hz, 1H), 2.10 (ddd, J = 10.1, 6.7, 3.2 Hz, 1H), 1.91 (d, J = 1.2 Hz, 3H), 1.82 – 1.56 (m, 4H), 1.33 (dd, J = 10.5, 8.3 Hz, 1H), 1.14 (d, J = 6.9 Hz, 3H), 1.12 (s, 3H), 1.10 (s, 3H).

Synthesis of compound 1

To a 0 °C solution of lathyrol (120 mg, 0.36 mmol) and NaH (1.5 eq) in dry DMF was added dropwise propargyl bromide (1.2 eq) under N₂ atmosphere. The resulting mixture was stirred for 1-2 h at room temperature. Upon completion, EtOAc and brine were added. The organic layer was washed with NH₄Cl solution and brine, respectively, dried over anhydrous Na₂SO₄, filtered, evaporated, and purified by silica gel CC to afford compound **1** as colorless oil (45% yield). ¹H NMR (600 MHz, DMSO-*d*₆) δ 7.46 (s, 1H), 4.81 (d, J = 14.2 Hz, 1H), 4.64 (s, 1H), 4.53 (d, J = 8.4 Hz, 1H), 4.42 (s, 1H), 4.33 (qd, J = 15.8, 2.4 Hz, 2H), 4.24 (t, J = 9.1 Hz, 1H), 4.07 (s, 1H), 4.03 (t, J = 3.3 Hz, 1H), 2.80 (dd, J = 12.9, 9.0 Hz, 1H), 2.54 (dd, J = 13.3, 6.8 Hz, 1H), 2.13 (dd, J = 9.8, 3.3 Hz, 1H), 2.01 – 1.82 (m, 4H), 1.55 (s, 3H), 1.53 – 1.37 (m, 4H), 1.17 (ddd, J = 12.2, 8.2, 4.3 Hz, 1H), 1.14 (s, 4H), 1.07 (s, 3H), 1.05 (d, J = 6.7 Hz, 3H), 0.99 (t, J = 7.4 Hz, 2H).

Synthesis of compound 3

Compound **2** was dissolved in DMF. Then DIPEA (2 eq) and NH₂-PEG3-N₃ (1 eq) were added to the solution. The mixture was stirred for 3 h at 90 °C. Upon completion, EtOAc and brine were added. The organic layers was washed with NH₄Cl solution and brine, respectively, dried over anhydrous Na₂SO₄, and then filtered, evaporated, and purified by silica gel CC to obtain compound **3** as dark green solid (30% yield). ¹H NMR (600 MHz, CDCl₃) δ 8.29 (s, 1H), 7.49 (dd, J = 8.5, 7.1 Hz, 1H), 7.10 (d, J = 7.0 Hz, 1H), 6.93 (d, J = 8.5 Hz, 1H), 4.92 (dd, J = 12.4, 5.3 Hz, 1H), 3.73 (t, J = 5.5 Hz, 2H), 3.71 – 3.64 (m, 10H), 3.48 (t, J = 5.5 Hz, 2H), 3.42 – 3.32 (m, 2H), 2.95 – 2.66 (m, 3H), 2.17 – 2.06 (m, 1H).

Synthesis of compound 4 (ZCY-PROTAC)

To a solution of compound **1** (1.0 eq) and **3** (1.0 eq) in THF/H₂O (3/1) were added sodium ascorbate (0.8 eq) and CuSO₄ (0.4 eq) at room temperature. The mixture was then stirred for 20 minutes at room temperature. Upon completion, EtOAc and brine were added. The organic layer

was washed with brine, then dried over anhydrous Na₂SO₄, filtered, evaporated and purified by silica gel CC to obtain compound **4** as light green solid (50% yield). HR-MS(ESI) *m/z*: 847.4230 [M+H]⁺ (Calcd. for C₄₄H₅₉N₆O₁₁, 847.4236); ¹H NMR (600 MHz, DMSO-*d*₆) δ 11.11 (s, 1H), 8.04 (s, 1H), 7.98 (s, 1H), 7.63 – 7.51 (m, 1H), 7.14 (d, *J* = 8.6 Hz, 1H), 7.04 (d, *J* = 7.0 Hz, 1H), 6.60 (t, *J* = 5.4 Hz, 1H), 5.76 (s, 1H), 5.06 (dd, *J* = 12.9, 5.4 Hz, 1H), 4.74 (d, *J* = 11.9 Hz, 1H), 4.66 (d, *J* = 8.1 Hz, 1H), 4.53 – 4.43 (m, 3H), 4.35 (d, *J* = 9.5 Hz, 1H), 4.15 (s, 1H), 3.83 – 3.75 (m, 2H), 3.61 (dd, *J* = 8.7, 5.0 Hz, 2H), 3.56 – 3.53 (m, 2H), 3.52 – 3.43 (m, 9H), 2.86 (ddd, *J* = 38.7, 20.1, 8.6 Hz, 2H), 2.57 (dd, *J* = 27.0, 15.4 Hz, 2H), 2.17 (dd, *J* = 9.3, 2.8 Hz, 1H), 2.07 – 1.79 (m, 4H), 1.56 (s, 2H), 1.48 (dd, *J* = 28.2, 15.7 Hz, 2H), 1.43 – 1.37 (m, 1H), 1.20 – 1.14 (m, 1H), 1.13 (s, 3H), 1.10 (s, 1H), 1.05 (s, 2H), 1.01 (d, *J* = 6.7 Hz, 1H), 0.95 (d, *J* = 6.6 Hz, 2H). ¹³C NMR (150 MHz, DMSO-*d*₆) δ 202.16, 173.26, 170.52, 169.40, 167.75, 150.20, 146.86, 145.94, 145.31, 144.85, 136.68, 133.91, 132.55, 124.31, 117.89, 113.05, 111.14, 110.24, 109.70, 88.32, 70.23, 70.18, 70.03, 69.34, 69.22, 65.67, 61.34, 56.28, 55.37, 50.10, 49.81, 49.02, 42.16, 38.04, 35.93, 31.45, 28.99, 28.47, 25.36, 22.62, 22.12, 16.66, 15.10, 15.07, 12.93.

Cell culture and chemicals

Mouse RAW264.7 macrophage and human embryonic kidney 293T (HEK293T) cells were obtained from ATCC and grown in Dulbecco's modified Eagle's medium (DMEM, GIBCO) complemented with 10% fetal bovine serum (FBS, GIBCO), 100 U/mL penicillin and 100 µg/mL streptomycin (Hyclone) and at 37 °C in a humidified atmosphere with 5% CO₂. To induce inflammatory response, RAW264.7 cells were pretreated with compounds alone or in combination with 5 µM ML385 (MCE, #HY-100523) or 5 mM N-acetyl-L-cysteine (NAC, Beyotime, #S0077) for 2 h, and then incubated with 1 µg/mL Lipopolysaccharide (LPS, Sigma-Aldrich, #L2880) for 24 h. For all PROTAC treatment, unless otherwise stated, cells were incubated with chemicals for 48 h. For proteasome inhibition assay, cells were pretreated with PROTAC for 12 h following by MG132 (MCE, #HY13259) for 12 h. For ligand competition experiment, cells were administrated with PROTAC together with excess Lathyrol or thalidomide for 48 h.

Mass spectrometry for proteomics

RAW264.7 cells were incubated with ZCY-PROTAC or DMSO for 48 h, collected and resuspended in lysis buffer (8 M urea, 2 mM EDTA, 10 mM DTT and 1% protease inhibitor cocktail). Protein was extracted by ultrasonic (5 x 6 s) and centrifugation at 12,000 g for 10 min at 4 °C, and the protein concentration was quantified by BCA assay. The protein was precipitated with cold 20% Trichloroacetic for 2 h at 4 °C. After centrifugation at 4500 g for 5 min, the precipitate was washed for 3 times with cold acetone. The protein pellets were resuspended with 200 mM triethylammonium bicarbonate (TEAB) buffer and digested by trypsin (1: 50) overnight.

After trypsin digestion, peptides were desalted by Strata X (Phenomenex) and vacuum-dried. The peptides were dissolved with 0.5 M TEAB and labeled according to the operation instructions of the 6-plex (Tandem Mass Tag) TMT kit. The peptides were separated by a reversed-phase analytical column using a mix of buffer A (0.1% formic acid and 2% acetonitrile in water) and B (0.1% formic acid and 90% acetonitrile) on EASY-nLC 1000 UPLC system (Thermo Scientific). The separated peptides were implanted into nanospray-ionization (NSI) and then analyzed by tandem mass spectrometry (MS/MS) in a Q Exactive Plus (Thermo Scientific) coupled online to the UPLC. Intact peptides and the secondary fragments were detected and analyzed by high-resolution

Orbitrap. The electrospray voltage was set as 2.0 kV.

The MS/MS data were processed using the Mascot search engine (v.2.3.0), and matched in the proteome database. Trypsin/P was specified as the cleavage enzyme, allowing up to 2 missing cleavages and a minimum peptide length of 7 amino acid residues. The mass error was set to 10 ppm for precursor ions and 0.02 Da for fragment ions. Alkylation of cysteine residues was set as a fixed modification, and methionine oxidation was set as a variable modification. The data was filtered by a 1% false discovery rate (FDR). Quantified proteins were filtered if the absolute fold-change difference ≥ 1.5 .

Immunoblot (IB) and immunofluorescence (IF) assay

For IB, collected cells were resuspended in radioimmunoprecipitation assay (RIPA) lysis buffer (Beyotime, #P0013B) supplemented with 1 mM Phenylmethylsulfonyl fluoride (PMSF, Roche, #329-98-6) and kept on ice for 30 min, and then centrifuged 10 min at 13,000 rpm. The total protein content was measured by bicinchoninic acid (BCA) Kit (Beyotime, #P0012). The lysate protein (20-40 μ g) was separated by sodium dodecyl sulfate polyacrylamide gel electrophoresis (SDS-PAGE) and electrophoretically transferred to poly (vinylidene difluoride) (PVDF) membranes (Millipore, #IPVH00010), which were sequentially subjected to specific primary antibody (1:1000) and HRP-conjugated secondary antibody (1:5000), respectively. The bands were finally visualized by the Tanon-5200 Chemiluminescent Imaging System with ECL luminescence reagents (Beyotime, #P0018M).

For IF, the cells were fixed in 4% paraformaldehyde in phosphate buffered solution (PBS) for 20 min, incubated with 0.2% Triton X-100 for 15 min, and blocked with 5% BSA for 1 h. The cells were then incubated with specific primary antibody (1:500) at 4 °C overnight and sequentially incubated with Fluorescent secondary antibody (1:500). Images were obtained by a Zeiss Observer.Z1 fluorescent microscope using the Slidebook 4.2.0.11 software (Intelligent Imaging Innovations, Inc.).

Primary antibodies were used in this studies as follows: MAFF (Proteintech, #12771-1-AP), Nrf2 (Proteintech, #16396-1-AP), Keap1 (Proteintech, #10503-2-AP), HO-1 (Proteintech, #27282-1-AP), I κ B α (ABclonal, #A11397), p-I κ B α (ABclonal, #AP0707), NF- κ B p65 (Proteintech, #10745-1-AP), iNOS (Proteintech, #22226-1-AP), COX-2 (Proteintech, #12375-1-AP), LC3B (ABclonal, #A19665), BNIP3 (Proteintech, #12986-1-AP), P62 (Proteintech, #18420-1-AP), β -Actin (ABclonal, #AC026), HA-tag (Proteintech, #51064-2-AP), FLAG-tag (Proteintech, #20543-1-AP), GST-tag (Proteintech, #10000-0-AP), HIS-tag (Proteintech, #66005-1-Ig). Secondary antibodies for IB and IF were listed below: horseradish peroxidase (HRP)-conjugated goat anti-rabbit IgG (H+L) (Proteintech, #SA00001-2), HRP-conjugated goat anti-mouse IgG (H+L) (Proteintech, #SA00001-1), CoraLite488-conjugated goat anti-rabbit or anti-mouse IgG (H+L) (Proteintech, #SA00013-2 or SA00013-1), Cy3-conjugated goat anti-rabbit IgG (H+L) (Proteintech, #SA00009-2).

Immunoprecipitation (IP) analysis

For endogenous immunoprecipitation, RAW264.7 cell lysates were obtained in immunoprecipitation assay buffer (Beyotime, #P0013) containing 1 mM PMSF. The cell lysates were pre-cleared with 10 μ L of protein A+G agarose beads (Beyotime, #P2055) for 1 h. After that, the cell lysates were incubated with 1 μ g of specific antibody on a rotator at 4 °C overnight, and then incubated with 20 μ L of protein A+G agarose beads for 4 h. The IP complexes were washed

for five times with PBS and eluted in sample buffer (50 mM Tris-HCl, pH 6.9, 2% SDS, 10% glycerol, 100 mM DTT, 0.1% bromophenol blue) by boiling for 5 min. Samples were then subjected to SDS-PAGE for immunoblot analysis. For immunoprecipitation of overexpressed protein, HEK293T cells were transfected with vectors expressing MAFF-GFP-HA, Nrf2-FLAG, MAFK-GST and MAFG-HIS. After 48 h transfection, the cell lysates were obtained in immunoprecipitation assay buffer and immunoprecipitated as above.

mRNA extraction and real-time qRT-PCR analysis

Total mRNA was extracted using TRIzol (Sigma-Aldrich, #T9424) according to the manufacturer's instructions. cDNA was then synthesized from 1 µg of mRNA by using the PrimeScript™ RT reagent Kit (TaKaRa, #RR037A). Real-time quantitative PCR (qRT-PCR) was then performed using TB Green Premix Ex Taq™ II (TaKaRa, #RR820A). The β-Actin gene (*ACTB*) was used to normalize relative mRNA levels. Primer sequences are as follows:

Mouse-*HMOX1*-Forward: 5' - AGGCTAAGACCGCCTTCCT - 3'

Mouse-*HMOX1*-Reverse: 5' - TGTGTTCTCTGTCAGCATCA - 3'

Mouse-*NQO1*-Forward: 5' - AGCGTTCGGTATTACGATCC - 3'

Mouse-*NQO1*-Reverse: 5' - AGTACAATCAGGGCTCTTCTCG - 3'

Mouse-*GCLM*-Forward: 5' - TGGAGCAGCTGTATCAGTGG - 3'

Mouse-*GCLM*-Reverse: 5' - CAAAGGCAGTCAAATCTGGTG - 3'

Mouse-*GCLC*-Forward: 5' - AGATGATAGAACACGGGAGGAG - 3'

Mouse-*GCLC*-Reverse: 5' - TGATCCTAAAGCGATTGTTCTTC - 3'

Mouse-*IL-6*-Forward: 5' - GCTACCAAACCTGGATATAATCAGGA - 3'

Mouse-*IL-6*-Reverse: 5' - CCAGGTAGCTATGGTACTCCAGAA - 3'

Mouse-*IL-1β*-Forward: 5' - AGCTTCAGGCAGGCAGTATC - 3'

Mouse-*IL-1β*-Reverse: 5' - GTCACAGAGGATGGGCTCTT - 3'

Mouse-*TNF*-Forward: 5' - TCTTCTCATTCTGCTTGTGG - 3'

Mouse-*TNF*-Reverse: 5' - GGTCTGGGCCATAGAAGTGA - 3'

Mouse- *ACTB* -Forward: 5' - AAGGCCAACCGTGAAAAGAT - 3'

Mouse- *ACTB* -Reverse: 5' - GTGGTACGACCAGAGGCATAC - 3'

Small interfering RNA transfection

Mouse short hairpin RNA (shRNA) vector for MAFF protein (shMAFF) was purchased from GENECHEM (#GIEE0272150). RAW264.7 cells were transfected with shRNA using Hieff Trans™ Liposomal Transfection Reagent (YEASEN, #40802ES03) according to the manufacturer's instructions. After 48 h posttransfection, cells were then used for immunoblot assays.

Nitric oxide (NO) detection assay

The production of NO was measured as previously reported [14]. RAW264.7 cells were seeded into 96-well plates with 1×10^4 cells per well and cultured for 24 h. Fresh medium containing series concentrations of compounds was replaced and incubated for 2 h. LPS (1 µg/mL) was added and then cells were kept incubating for 24 h. The supernatant samples were collected and measured by Griess reagent (Beyotime, #S0021S) at 540 nm. The inhibition of compounds on LPS-induced NO release was calculated by IC₅₀ value.

Cellular thermal shift assay (CETSA)

The ability of compounds to bind with and stabilize the target MAFF *in vitro* was assessed by cellular thermal shift assay. RAW264.7 cells were treated with DMSO or compounds (40 μ M) for 4 h and then collected and resuspended in PBS. The cell suspension was aliquoted into six PCR tubes and heated for 10 minutes to 64, 66, 68, 70, 72 or 74 °C. Then the samples were lysed using liquid nitrogen and two repeated cycles of freeze-thaw. After centrifuged at 13,000 g for 10 min at 4 °C, the supernatant was collected for further immunoblot analysis.

Drug affinity responsive target stability (DARTS) assay

The cells were collected and total protein was isolated using RIPA lysis buffer. The lysates were 1:10 diluted with TNC buffer (50 mM Tris-HCl, pH 8.0, 50 mM NaCl, 10 mM CaCl₂) and treated with 10, 20 or 40 μ M of compounds or DMSO as control. After incubation for 1 h at room temperature, pronase E (Sigma-Aldrich, #P5147) was added into the lysates for a further 15 min at 37 °C. Reactions were ceased by adding the sample buffer and boiling for 5 min and then analyzed via immunoblot analysis.

Expression and purification of MAFF

His-tagged human MAFF was transformed into *Escherichia coli* strain (BL21 DE3) and overexpressed at 37 °C to an A600 of 0.6-0.8. To induce expression, 0.5 mM isopropyl-1-thio-D-galactopyranoside (IPTG) was added, and *E. coli* cells were grown at 20 °C for 16-18 h. Cells were collected by centrifugation at 3000 g for 10 min and resuspended lysis buffer (50 mM sodium phosphate, pH 7.2, 250 mM NaCl, 5 mM imidazole, and 1 mM β -mercaptoethanol) and lysed by sonication, and then purified by nickel resin affinity chromatography. SIRT6 protein fractions were further purified using a HiTrap SP-Sepharose Fast Flow column with a linear gradient from 50 to 750 mM NaCl in 50 mM sodium phosphate, pH 7.2, and 1 mM β -mercaptoethanol. Fractions containing purified MAFF were pooled, concentrated, and stored at -80 °C.

Microscale thermophoresis (MST) assay

To explore the binding affinity of compounds with purified human MAFF protein, MST assay was performed as described [78]. The protein was labeled with the Monolith NTTM Protein Labeling Kit RED (# L001). Labeled MAFF was then diluted to 200 nM with assay buffer containing 20 mM HEPES (pH 7.5) and 0.05% (v/v) Tween-20. Compounds were diluted in a series of concentration and incubated with MAFF for 10 min at room temperature. Samples were loaded into Monolith standard-treated capillaries and the thermophoresis was performed at 25 °C on a Monolith NT.115 instrument (Nano Temper Technologies, München, Germany). Data were obtained with 100% light-emitting diode (LED) power. The dissociation constant K_D values were fitted by using the NT Analysis software (Nano Temper Technologies, München, Germany) .

Enzyme linked immunosorbent assay (ELISA)

To detect the release level of inflammatory cytokines IL-1 β , IL-6 and TNF- α , the supernatant of RAW264.7 cells and animal serum samples were applied to detect the content of IL-1 β , IL-6 and TNF- α by the commercial ELISA kits (Boster, #EK0394, #EK0411 and #EK0527), according to the manufacturer's instructions.

Measurement of intracellular ROS and mitochondrial superoxide (mtSOX)

RAW264.7 cells were pre-treated with compounds for 2h and then triggered with 1 µg/mL LPS for 24 h. Culture supernatants were removed and replaced with PBS containing 10 µM of DCFH-DA (Beyotime, #S0033S) for ROS detection or 5 µM of MitoSOX™ Red superoxide indicator (Invitrogen, #M36008) for mtSOX detection. After incubation for 20 min at 37 °C, cells were washed with PBS for three times, and then collected for flow cytometry analysis.

Animals

BALB/C mice (7-8 weeks) were purchased from the Laboratory Animal Center of Tongji Medical College of Huazhong University of Science and Technology (Wuhan, China). All animals were acclimated for 7 days before experiments and handled according with the Guide for the Care and Use of Laboratory Animals of Tongji Medical College, Huazhong University of Science and Technology and agreed by the Ethics Committee.

LPS-induced acute lung injury (ALI) mouse model

To evaluate the effect of ZCY020 on the survival of mice with LPS-induced acute lung injury (15 mg/kg, i.p.), Male BALB/C mice at 7–8 weeks were randomly divided into four groups (n=10 per group): the control group (saline, i.g.), LPS model group (LPS + saline, i.g.), low dose group (LPS + ZCY020 at 50 mg/kg, i.g.) and high dose group (LPS + ZCY020 at 100 mg/kg, i.g.). The saline or ZCY020 was administrated at 2 h before injection of LPS and at 12, 24, 48, 72 and 96 h after the injection of LPS. Survival was monitored daily for up to 1 week. During the experiment and at day 8, liver and spleen tissues were collected and fixed in 10% formalin and sections were stained with hematoxylin and eosin. Lungs were collected and divided as follows: two thirds were snap frozen in liquid nitrogen for total RNA extraction and protein assays, the other third was fixed with 10% buffered formalin, then embedded in paraffin for histological analyses.

To further evaluate the effect of ZCY020 on the production of LPS-induced pro-inflammatory cytokines, cytokines levels were assessed by measuring serum concentrations. 40 mice were randomly assigned into four groups as above: the control, LPS model and ZCY020 (50, 100 mg/kg) groups. Mice in LPS model group and ZCY020 treated groups were oral administrated with saline or ZCY020, and 90 min later, intraperitoneally injected with LPS at 1.5 mg/kg. Mice were sacrificed and serum samples were collected at 4 h after LPS administration. The concentrations of cytokines IL-1β and IL-6 were measured by sandwich ELISA using commercially available reagents according to the manufacturer's instructions. For each group, serum samples were obtained from at least six mice and analyzed in duplicate.

Statistical analysis

All results data are presented as mean ± SD for at least three independent experiments. Statistical analysis was performed using GraphPad Prism 7.0 and SPSS 21.0. Data were analyzed by unpaired Student's *t*-test between 2 groups, and one-way ANOVA with Tukey's test was applied to determine the statistical significance of more than 2 groups. *p* < 0.05 was considered statistically significant.

Data Availability

All study data and figures are included in the article and/or supporting information.

Acknowledgements

This work was supported by National Natural Science Foundation of China (NSFC) (No. 81773594, 81773637, U1803122, U1703111), Chunhui Program-Cooperative Research Project of the Ministry of Education, Wuhan COVID-19 Emergency Research Fund (grant number EX20C02), Liaoning Revitalization Talents Program (No. XLYC1807182), and Liaoning Province Natural Science Foundation (No. 2019-MS-299, 2020-MZLH-31).

Appendix. Supplementary Information

REFERENCES

1. A. C. Lai, C. M. Crews, Induced protein degradation: an emerging drug discovery paradigm. *Nat. Rev. Drug Discov.* 16, 101-114 (2017).
2. H. Inuzuka, J. Liu, W. Wei, A. Rezaeiana. PROTAC technology for the treatment of Alzheimer's disease: advances and perspectives. *Acta Materia Medica.* 1, 24-41 (2022).
3. R. J. Deshaies, Protein degradation: Prime time for PROTACs. *Nat. Chem. Biol.* 11, 634-635 (2015).
4. S. Zeng *et al.*, Proteolysis targeting chimera (PROTAC) in drug discovery paradigm: Recent progress and future challenges. *Eur. J. Med. Chem.* 210, 112981 (2021).
5. G. M. Burslem, C. M. Crews, Proteolysis-Targeting Chimeras as Therapeutics and Tools for Biological Discovery. *Cell* 181, 102-114 (2020).
6. J.B. Baell, Feeling Nature's PAINS: Natural Products, Natural Product Drugs, and Pan Assay Interference Compounds (PAINS). *J. Nat. Prod.* 79, 616-628 (2016).
7. Y. Li *et al.*, Identification of PDE6D as a potential target of sorafenib via PROTAC technology. bioRxiv [Preprint] (2020). <https://doi.org/10.1101/2020.05.06.079947>
8. A. Vasas, J. Hohmann, Euphorbia diterpenes: isolation, structure, biological activity, and synthesis (2008-2012). *Chem. Rev.* 114, 8579-8612 (2014).
9. Y. Xu *et al.*, Diterpenoids from the genus Euphorbia: Structure and biological activity (2013-2019). *Phytochemistry* 190, 112846 (2021).
10. A. Zhu, T. Zhang, Q. Wang. The phytochemistry, pharmacokinetics, pharmacology and toxicity of Euphorbia semen. *J. Ethnopharmacol.* 227, 41-55 (2018).
11. J. Lu *et al.*, Lathyrane-type diterpenoids from the seeds of *Euphorbia lathyris*. *Phytochemistry* 104, 79-88 (2014).
12. J.X. Wang *et al.*, Cytotoxic lathyrane-type diterpenes from seeds of *Euphorbia Lathyris*. *Chem. Pharm. Bull. (Tokyo)* 66, 674-677 (2018).
13. Q. W. Shi, X. H. Su, H. Kiyota, Chemical and pharmacological research of the plants in genus Euphorbia. *Chem. Rev.* 108, 4295-4327 (2008).
14. C. Y. Zhang *et al.*, Anti-inflammatory Lathyrane Diterpenoids from *Euphorbia lathyris*. *J. Nat. Prod.* 82, 756-764 (2019).
15. Y. Wang *et al.*, Diterpenoids from the seeds of *Euphorbia lathyris* and their anti-inflammatory activity. *Bioorg. Chem.* 112, 104944 (2021).
16. A. Zhu, T. Zhang, Q. Wang, The phytochemistry, pharmacokinetics, pharmacology and toxicity of *Euphorbia* semen. *J. Ethnopharmacol.* 227, 41-55 (2018).

17. Q. P. Zhang *et al.*, Euphorbia factor L2 alleviates lipopolysaccharide-induced acute lung injury and inflammation in mice through the suppression of NF- κ B activation. *Biochem. Pharmacol.* 155, 444-454 (2018).
18. M. Nishizawa, K. Kataoka, N. Goto, K. T. Fujiwara, S. Kawai, v-maf, a viral oncogene that encodes a "leucine zipper" motif. *Proc. Natl. Acad. Sci. U. S. A.* 86, 7711–7715 (1989).
19. F. Katsuoka, M. Yamamoto, Small Maf proteins (MafF, MafG, MafK): History, structure and function. *Gene* 586, 197-205 (2016).
20. K. Kataoka *et al.*, Small Maf proteins heterodimerize with Fos and may act as competitive repressors of the NF-E2 transcription factor. *Mol. Cell. Biol.* 15, 2180–2190 (1995).
21. K. Igarashi *et al.*, Regulation of transcription by dimerization of erythroid factor NF-E2 p45 with small Maf proteins. *Nature* 367, 568–572 (1994).
22. T. Oyake *et al.*, Bach proteins belong to a novel family of BTB-basic leucine zipper transcription factors that interact with MafK and regulate transcription through the NF-E2 site. *Mol. Cell. Biol.* 16, 6083–6095 (1996).
23. K. Itoh *et al.*, An Nrf2/small Maf heterodimer mediates the induction of phase II detoxifying enzyme genes through antioxidant response elements. *Biochem. Biophys. Res. Commun.* 236, 313–322 (1997).
24. O. Johnsen, P. Murphy, H. Prydz, A. B. Kolsto, Interaction of the CNC-bZIP factor TCF11/LCR-F1/Nrf1 with MafG: binding-site selection and regulation of transcription. *Nucleic Acids Res.* 26, 512-520 (1998).
25. A. Kobayashi *et al.*, Molecular cloning and functional characterization of a new Cap'n' collar family transcription factor Nrf3. *J. Biol. Chem.* 274, 6443-6452 (1999).
26. J. A. Moran, E. L. Dahl, R. T. Mulcahy, Differential induction of maff, mafG and mafK expression by electrophile-response-element activators. *Biochem. J.* 361, 371-377 (2002).
27. H. Motohashi, F. Katsuoka, J. A. Shavit, J. D. Engel, M. Yamamoto, Positive or negative MARE-dependent transcriptional regulation is determined by the abundance of small Maf proteins. *Cell* 103, 865-875 (2000).
28. W. Massrieh *et al.*, Regulation of the MAFF transcription factor by proinflammatory cytokines in myometrial cells. *Biol. Reprod.* 74, 699-705 (2006).
29. J. Saliba, B. Coutaud, V. Solovieva, F. Lu, V. Blank, Regulation of CXCL1 chemokine and CSF3 cytokine levels in myometrial cells by the MAFF transcription factor. *J. Cell. Mol. Med.* 23, 2517-2525 (2019).
30. X. Wang *et al.*, Responsive Expression of Maff to β -Amyloid-Induced Oxidative Stress. *Dis. Markers* 2020, 8861358 (2020).
31. M. von Scheidt *et al.*, Transcription Factor MAFF (MAF Basic Leucine Zipper Transcription Factor F) Regulates an Atherosclerosis Relevant Network Connecting Inflammation and Cholesterol Metabolism. *Circulation* 143, 1809-1823 (2021).
32. S. D. Field *et al.*, Fluorophosphonate-Based Degradable Serine Hydrolases by Quantitative Proteomics. *Chembiochem.* 21, 2916-2920 (2020).
33. T. Suzuki, M. Yamamoto, Molecular basis of the Keap1-Nrf2 system. *Free Radic. Biol. Med.* 88, 93-100 (2015).
34. T. W. Kensler, N. Wakabayashi, S. Biswal, Cell survival responses to environmental stresses via the Keap1-Nrf2-ARE pathway. *Annu. Rev. Pharmacol. Toxicol.* 47, 89-116 (2007).
35. H. Motohashi *et al.*, MafG sumoylation is required for active transcriptional repression. *Mol.*

- Cell. Biol.* 26, 4652-4663 (2006).
36. C. Tonelli, I. Chio, D. A. Tuveson, Transcriptional Regulation by Nrf2. *Antioxid. Redox Signal.* 29, 1727-1745 (2018).
 37. C. A. Piantadosi, M. S. Carraway, A. Babiker, H. B. Suliman, Heme oxygenase-1 regulates cardiac mitochondrial biogenesis via Nrf2-mediated transcriptional control of nuclear respiratory factor-1. *Circ. Res.* 103, 1232-1240 (2008).
 38. S. M. Ahmed, L. Luo, A. Namani, X. J. Wang, X. Tang, Nrf2 signaling pathway: Pivotal roles in inflammation. *Biochim. Biophys. Acta Mol. Basis Dis.* 1863, 585-597 (2017).
 39. N. K. Campbell, H. K. Fitzgerald, A. Dunne, Regulation of inflammation by the antioxidant haem oxygenase 1. *Nat. Rev. Immunol.* 21, 411-425 (2021).
 40. A. A. Waza, Z. Hamid, S. Ali, S. A. Bhat, M. A. Bhat, A review on heme oxygenase-1 induction: is it a necessary evil. *Inflamm. Res.* 67, 579-588 (2018).
 41. R. Gozzelino, V. Jeney, M. P. Soares, Mechanisms of cell protection by heme oxygenase-1. *Annu. Rev. Pharmacol. Toxicol.* 50, 323-354 (2010).
 42. H. G. Chen *et al.*, Heme oxygenase-1 mediates the anti-inflammatory effect of molecular hydrogen in LPS-stimulated RAW 264.7 macrophages. *Int. J. Surg.* 11, 1060-1066 (2013).
 43. M. H. Kapturczak *et al.*, Heme oxygenase-1 modulates early inflammatory responses: evidence from the heme oxygenase-1-deficient mouse. *Am. J. Pathol.* 165, 1045-1053 (2004).
 44. X. Chi *et al.*, Elevation of HO-1 Expression Mitigates Intestinal Ischemia-Reperfusion Injury and Restores Tight Junction Function in a Rat Liver Transplantation Model. *Oxid. Med. Cell. Longev.* 2015, 986075 (2015).
 45. T. Hussain *et al.*, Oxidative Stress and Inflammation: What Polyphenols Can Do for Us? *Oxid. Med. Cell. Longev.* 2016, 7432797 (2016).
 46. A. Singh *et al.*, Small Molecule Inhibitor of NRF2 Selectively Intervenes Therapeutic Resistance in KEAP1-Deficient NSCLC Tumors. *ACS Chem. Biol.* 11, 3214-3225 (2016).
 47. J. D. Wardyn, A. H. Ponsford, C. M. Sanderson, Dissecting molecular cross-talk between Nrf2 and NF- κ B response pathways. *Biochem. Soc. Trans.* 43, 621-626 (2015).
 48. M. P. Soares *et al.*, Heme oxygenase-1 modulates the expression of adhesion molecules associated with endothelial cell activation. *J. Immunol.* 172, 3553-3563 (2004).
 49. W. Lin *et al.*, Sulforaphane suppressed LPS-induced inflammation in mouse peritoneal macrophages through Nrf2 dependent pathway. *Biochem. Pharmacol.* 76, 967-973 (2008).
 50. J. A. DiDonato, F. Mercurio, M. Karin, NF- κ B and the link between inflammation and cancer. *Immunol. Rev.* 246, 379-400 (2012).
 51. T. Yu, J. L. Robotham, Y. Yoon, Increased production of reactive oxygen species in hyperglycemic conditions requires dynamic change of mitochondrial morphology. *Proc. Natl. Acad. Sci. U. S. A.* 103, 2653-2658 (2006).
 52. L. A. Sena, N. S. Chandel, Physiological roles of mitochondrial reactive oxygen species. *Mol. Cell* 48, 158-167 (2012).
 53. M. Lazarou, Keeping the immune system in check: a role for mitophagy. *Immunol. Cell. Biol.* 93, 3-10 (2015).
 54. L. Xiao *et al.*, The mitochondria-targeted antioxidant MitoQ ameliorated tubular injury mediated by mitophagy in diabetic kidney disease via Nrf2/PINK1. *Redox Biol.* 11, 297-311 (2017).

55. I. G. Ryoo, M. K. Kwak, Regulatory crosstalk between the oxidative stress-related transcription factor Nfe2l2/Nrf2 and mitochondria. *Toxicol. Appl. Pharmacol.* 359, 24-33 (2018).
56. T. C. Kang, Nuclear Factor-Erythroid 2-Related Factor 2 (Nrf2) and Mitochondrial Dynamics/Mitophagy in Neurological Diseases. *Antioxidants (Basel)* 9, 617 (2020).
57. M. L. Seibenhener *et al.*, A role for sequestosome 1/p62 in mitochondrial dynamics, import and genome integrity. *Biochim. Biophys. Acta* 1833, 452-459 (2013).
58. M. L. Seibenhener *et al.*, Behavioral effects of SQSTM1/p62 overexpression in mice: support for a mitochondrial role in depression and anxiety. *Behav. Brain Res.* 248, 94-103 (2013).
59. M. Onishi, K. Yamano, M. Sato, N. Matsuda, K. Okamoto, Molecular mechanisms and physiological functions of mitophagy. *EMBO J.* 40, e104705 (2021).
60. X. Lin, M. Wei, F. Song, D. I. Xue, Y. Wang, N-acetylcysteine (NAC) Attenuating Apoptosis and Autophagy in RAW264.7 Cells in Response to Incubation with Mycolic Acid from Bovine Mycobacterium tuberculosis Complex. *Pol. J. Microbiol.* 69, 223-229 (2020).
61. D. Fu *et al.*, Costunolide Induces Autophagy and Apoptosis by Activating ROS/MAPK Signaling Pathways in Renal Cell Carcinoma. *Front. Oncol.* 10, 582273 (2020).
62. T. Dong *et al.*, Ainsliadimer A selectively inhibits IKK α/β by covalently binding a conserved cysteine. *Nat. Commun.* 6, 6522 (2020).
63. J. Ha, H. Park, J. Park, S. B. Park, Recent advances in identifying protein targets in drug discovery. *Cell Chem. Biol.* 28, 394-423 (2021).
64. B. F. Cravatt, A. T. Wright, J. W. Kozarich, Activity-based protein profiling: from enzyme chemistry to proteomic chemistry. *Annu. Rev. Biochem.* 77, 383-414 (2008).
65. M. J. Niphakis, B. F. Cravatt, Enzyme inhibitor discovery by activity-based protein profiling. *Annu. Rev. Biochem.* 83, 341-377 (2014).
66. L. Burdine, T. Kodadek, Target identification in chemical genetics: the (often) missing link. *Chem. Biol.* 11, 593-597 (2004).
67. Y. Qu *et al.*, Axitinib blocks Wnt/ β -catenin signaling and directs asymmetric cell division in cancer. *Proc. Natl. Acad. Sci. U. S. A.* 113, 9339-9344 (2016).
68. M. M. Savitski *et al.*, Tracking cancer drugs in living cells by thermal profiling of the proteome. *Science* 346, 1255784 (2014).
69. D. P. Bondeson *et al.*, Lessons in PROTAC Design from Selective Degradation with a Promiscuous Warhead. *Cell Chem. Biol.* 25, 78-87 (2018).
70. H. T. Huang *et al.*, A Chemoproteomic Approach to Query the Degradable Kinome Using a Multi-kinase Degradator. *Cell Chem. Biol.* 25, 88-99 (2018).
71. Y. Xu, J. Shen, Z. Ran, Emerging views of mitophagy in immunity and autoimmune diseases. *Autophagy* 16, 3-17 (2020).
72. M. Komatsu *et al.*, The selective autophagy substrate p62 activates the stress responsive transcription factor Nrf2 through inactivation of Keap1. *Nat. Cell Biol.* 12, 213-223 (2010).
73. Y. Ichimura *et al.*, Phosphorylation of p62 activates the Keap1-Nrf2 pathway during selective autophagy. *Mol. Cell* 51, 618-631 (2013).
74. R. Blank, L. M. Napolitano, Epidemiology of ARDS and ALI. *Crit. Care Clin.* 27, 439-458 (2011).
75. A. Urakov, N. Urakova, K. Gurevich, N. Muhutdinov. Cardiology, respiratory failure, and tolerance of hypoxia in the context of COVID-19: a multidisciplinary perspective. *Rev Cardiovasc Med.* 17, 23:21 (2022).

76. J. R. Tisoncik *et al.*, Into the eye of the cytokine storm. *Microbiol. Mol. Biol. Rev.* 76, 16-32 (2012).
77. C. Li *et al.*, Corticosteroid treatment ameliorates acute lung injury induced by 2009 swine origin influenza A (H1N1) virus in mice. *PLoS One* 7, e44110 (2012).
78. C. J. Wienken, P. Baaske, U. Rothbauer, D. Braun, S. Duhr, Protein-binding assays in biological liquids using microscale thermophoresis. *Nat. Commun.* 1, 100 (2010).